The exchange of Intermediate Water in the southeast Atlantic: Water mass transformations diagnosed from the Lagrangian analysis of a regional ocean model

Julie Rimaud,[1] Sabrina Speich,[1] Bruno Blanke,[1] and Nicolas Grima[1]

Received 18 March 2012; revised 7 June 2012; accepted 11 June 2012; published 25 August 2012.

[1] Results from a regional ocean model and numerical Lagrangian analyses are compared with in situ measurements to describe the properties and dynamics of Antarctic Intermediate Water (AAIW) in the region of the Cape Basin. The AAIW that originates in the South Atlantic (A-AAIW) at 8°W follows two branches. A southern branch, flowing mostly south of 40°S, is blocked by topography and is deflected westward without significant changes in its physical properties. A northern branch crosses the Cape Basin with strong modification of its physical properties. The AAIW that originates in the Indian Ocean (I-AAIW) flows into the Atlantic Ocean via the Agulhas Current and undergoes small physical changes in the Cape Basin. In the model, the salinity ranges of A-AAIW and I-AAIW cores that reach the southeast Atlantic are 34.2–34.5 and 34.5–34.6, respectively. The modeled AAIW distribution and behavior compare well with observations, despite a bias of +0.2 in salinity. To investigate the dynamical processes involved in the interocean exchanges of these AAIW varieties, we use diagnoses based on the Okubo-Weiss parameter and the directional variations of trajectories of particles transported by the model velocity field. Our results suggest that I-AAIW flows into the Cape Basin more within eddies, and particularly within cyclones, than A-AAIW. Once the mixing of both varieties operates, physical and behavioral differences fade and the resulting AAIW flows over the Walvis Ridge in a less turbulent way as part of the Benguela Current, with salinity between 34.55 and 34.6.

Citation: Rimaud, J., S. Speich, B. Blanke, and N. Grima (2012), The exchange of Intermediate Water in the southeast Atlantic: Water mass transformations diagnosed from the Lagrangian analysis of a regional ocean model, *J. Geophys. Res.*, *117*, C08034, doi:10.1029/2012JC008059.

1. Introduction

[2] An accurate description of the heat and freshwater fluxes across and between the atmosphere and the ocean is essential for understanding the current climate and its evolution. For this reason, ocean interbasin exchanges must be described and assessed thoroughly since they participate heavily in the heat and salt budget of each basin [*Gordon*, 2001]. Indeed, the global ocean is an engine redistributing heat and salinity globally within the global Meridional Overturning Circulation (MOC) [*Broecker*, 1987, 1991; *Lumpkin and Speer*, 2007; *Lumpkin et al.*, 2008]. Changes in haline and thermal properties of water masses, defining density through the equation of state for seawater, create horizontal pressure gradients that generate large-scale ocean movements. The MOC is a three-dimensional circulation pattern that links the main ocean basins and spans their full depth. Both wind- and buoyancy-forced circulations contribute to the MOC. The transport of properties by the MOC depends on the rate of overturning and the difference in property concentration between the upper and lower limbs of the overturning. In particular, the transformation of surface and thermocline water into deep water in the North Atlantic is balanced by the northward advection in the Atlantic of surface and thermocline water of Pacific, Indian and Atlantic origins. Hence, interhemispheric and interocean exchanges are of paramount importance within the MOC. South of Africa, these exchanges are complex and rely on large-scale density gradients, on the wind and on submesoscale and mesoscale processes [*Boebel et al.*, 2003; *Dencausse et al.*, 2010, 2011; *Arhan et al.*, 2011].

[3] The Southern Ocean, which surrounds Antarctica and extends north as far as 34°S, is a critical link. It controls climate to a large extent through the accentuation of various physical processes [*Toggweiler and Samuels*, 1998; *Rintoul et al.*, 2001; *Hallberg and Gnanadesikan*, 2006; *Watson and Garabato*, 2006; *Böning et al.*, 2008]. The intense regime of westerly winds over an open ocean almost free from any orographic barrier gives birth to the Antarctic Circumpolar Current (ACC), the most intense current in the

[1]Laboratoire de Physique des Océans, UMR 6523, CNRS-Ifremer-IRD-UBO, Brest, France.

Corresponding author: J. Rimaud, Laboratoire de Physique des Océans, UMR 6523, CNRS-Ifremer-IRD-UBO, 6 av. Le Gorgeu, CS 93837, FR-29238 Brest CEDEX 3, France. (julie.rimaud@univ-brest.fr)

0148-0227/12/2012JC008059

world's ocean. The ACC consists in several circumpolar jets or fronts that separate different geographic zones with distinct physical and biochemical properties [*Peterson and Stramma*, 1991; *Orsi et al.*, 1995; *Belkin and Gordon*, 1996; *Sokolov and Rintoul*, 2002, 2009a, 2009b; *Pollard et al.*, 2002; *Ito et al.*, 2005]. The ACC is generally described as a cluster of three circumpolar deep-reaching jets: from north to south, the Subantarctic Front (SAF), the Polar Front, and the Southern ACC Front. At its northern edge, the ACC domain is separated from the subtropics by the Subtropical Convergence that is also called Subtropical Front (STF).

[4] The ACC has a key role in the redistribution of heat and freshwater fluxes with the other basins since the physical structure of the MOC and its effectiveness in regulating climate depend particularly on the water mass exchanges with the Southern Ocean [*Rintoul et al.*, 2001; *Speich et al.*, 2001, 2007; *Olbers et al.*, 2004; *Sokolov and Rintoul*, 2007]. The upper branch of the Atlantic MOC (AMOC) originates in the southeast Atlantic, where the waters of the South Atlantic Current (SAC) merge with subantarctic waters and with the Agulhas Current (AC), the most intense western boundary current [*Duncan*, 1970; *Lutjeharms*, 2001, 2006] to form the Benguela Current [*Reid*, 1989; *Peterson and Stramma*, 1991; *de Ruijter et al.*, 1999; *Stramma and England*, 1999]. According to *Gordon et al.* [1992], the Benguela Current waters have indeed three sources: the SAC, the AC and the ACC.

[5] Antarctic Intermediate Water (AAIW) and the thermocline waters of the southeast Atlantic are also components of the upper branch of the AMOC. AAIW is characterized by a salinity minimum. It flows below the thermocline and north of the SAF, unlike the Subantarctic Mode Water (SAMW) that flows in the uppermost ocean layers [*McCartney*, 1977; *Talley*, 1996; *Hanawa and Talley*, 2001; *Schmid and Garzoli*, 2009]. AAIW can be found in all the oceans [*Piola and Georgi*, 1982]. The changes in properties of AAIW in the eastern South Atlantic are large in comparison with the central to western South Atlantic [*Piola and Georgi*, 1982]. The area south of Africa is known not to be a formation region of intermediate water; hence, the AAIW varieties observed locally must be advected by the ocean circulation from different source regions [*Jacobs and Georgi*, 1977]. Therefore, all the AAIW that is identified in this region must have remote origins. The intermediate water of the southeast Atlantic comes from Drake Passage (dAAIW), the south of the Indian Ocean (siAAIW), the Indonesian Seas, the Red Sea and a transformed end-member of the mixture of all these sources (aAAIW) [*You*, 2002; *You et al.*, 2003].

[6] The southern limit of the AAIW extension must be studied in relation with the SAF, a frontal area that presents strong lateral gradients in temperature, salinity, density, and sea level. Though the subduction mechanism that leads to the formation of AAIW is partly unknown, in situ measurements show that such a process is active from the Polar Front and may contribute to elucidate the transformation of SAMW into AAIW [*McCartney*, 1977; *Talley*, 1996; *Hanawa and Talley*, 2001; *Schmid and Garzoli*, 2009]. AAIW from the South Atlantic (A-AAIW) includes dAAIW, which flows from the southeast Pacific across Drake Passage and is modified in the Malvinas Current into A-AAIW [*McCartney*, 1977; *Piola and Gordon*, 1989; *You*, 2002; *You et al.*, 2003].

[7] Unfortunately, the physical properties and the location of the exchanges between the South Atlantic and Indian varieties of AAIW are not well enough known to allow quantifying unambiguously their influence on the global circulation and climate system. The complex dynamics in the Cape Basin and the induced mixing of waters increase the difficulty to differentiate AAIW varieties according to their origins on their entrance in the Benguela Current, since their nominal properties are rapidly lost [*Richardson and Garzoli*, 2003]. The region of the Cape Basin is indeed at the convergence of Indian Ocean waters carried by the AC, South Atlantic waters carried by the SAC, and Southern Ocean waters carried by the ACC. There, several AAIW varieties essential to the MOC have been identified from the Argo database [*Speich et al.*, 2012; E. Rusciano et al., Interocean exchanges and the spreading of Antarctic Intermediate Water south of Africa, submitted to *Journal of Geophysical Research*, 2012]. So far, AAIW has also been poorly represented in numerical models. Consequently, the characterization, origin, dynamics, and mixing of its different varieties are not yet well understood in this area. AAIW is characterized by a salinity minimum below the thermocline. After it is formed, this water mass subducts under the seasonal thermocline and is no longer in contact with the atmospheric forcing. It retains the physical properties that were set at the sea surface, and it is a long-distance supplier of salt, heat, and nutrients typical of its formation regions [*Sarmiento et al.*, 2004].

[8] In this study, we use a numerical model to improve our understanding of the characteristics and dynamics of the different AAIW varieties flowing into the southeast Atlantic. We take an interest in their evolution from their origins until their convergence in the Benguela Current. For this purpose, a high-resolution simulation run with a regional ocean model is analyzed with numerical Lagrangian experiments and compared to in situ data acquired within the international CLIVAR GoodHope and International Polar Year BONUS-GoodHope programs. The paper is structured as follows. Section 2 introduces the ocean model, the Lagrangian framework, and the analyses carried out with the Okubo-Weiss parameter and the directional variations of trajectories of numerical particles. In section 3, we compare our regional model to available in situ data and other published studies. Our Lagrangian results on the properties, transport and dynamics of the local AAIW varieties are given in section 4. They are discussed in section 5 in the light of published literature. Our conclusions are presented in section 6.

2. Materials and Methods

2.1. Ocean Model

[9] The numerical model used in this work is the Regional Ocean Modeling System (ROMS). It is a split-explicit, free-surface, primitive equations ocean model, based on the Boussinesq approximation and hydrostatic vertical momentum balance [*Shchepetkin and McWilliams*, 2005, 2009]. The simulation covers the ocean domain around Southern

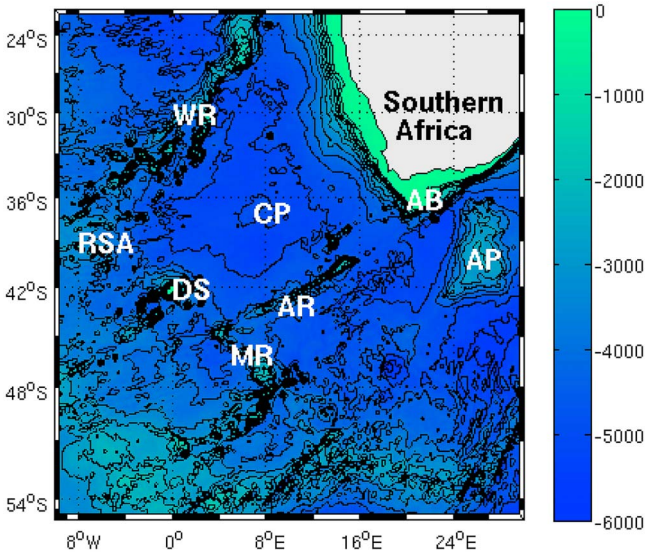

Figure 1. Seafloor bathymetry of the area of study with contours drawn every 500 m and with the following abbreviations for the main topographic features: WR = Walvis Ridge; CP = Cape Basin; RSA = RSA seamounts; DS = Discovery Seamounts; AR = Agulhas Ridge; AB = Agulhas Bank; MR = Meteor Rise; AP = Agulhas Plateau.

Africa from 55°S to 21.5°S and from 55°W to 34°E. Our study focuses on the region east of 10°W. The spatial resolution is 1/12° with 32 terrain-following vertical levels (with a higher resolution in the upper ocean layer). The bottom topography is derived from the ETOPO2 (2′ resolution) data set [*Smith and Sandwell*, 1997] and the area defined from 8°W to 30°E and from 25°S to 52°S displays a considerable relief with the Agulhas Bank (AB), the Agulhas Plateau (AP), and the Cape Basin (CP) surrounded by the Walvis Ridge (WR), the Agulhas Ridge (AR), the Republic of South Africa (RSA) Seamounts and the Discovery Seamounts (DS) (Figure 1). The model is run for 20 years driven by a monthly climatological wind stress derived from daily QuikSCAT satellite scatterometer data gridded at 1/2° resolution [*Institut Français de Recherche Pour l'Exploitation de la Mer and Centre ERS d'Archivage et de Traitement*, 2002]. The model is also forced by fresh water and radiative heat fluxes extracted from the Comprehensive Ocean-atmosphere Data Set (COADS) ocean surface monthly climatology at 1/2° resolution, whereas the latent and sensible heat fluxes use satellite-derived atmospheric quantities (air temperature and QuikSCAT wind) in their bulk formulation [*Bentamy et al.*, 2003; *Ayina et al.*, 2006]. All satellite-derived climatological fields were calculated with data available over 2000–2007. The model is forced at its open boundaries by climatological fields obtained from SODA (Simple Ocean Data Assimilation) [*Carton and Giese*, 2008]. The model solution is considered stable after a period of about 3 years, so the analysis will focus on the last 17 years of the simulation. Outputs are averaged and stored on a 2-day basis. To get insight into processes at fine scale, two months of the last year of the simulation were archived every 4 h. Pre- and post-processing of the simulation used the Matlab ROMSTOOLS toolbox (http://www.romsagrif.org/) [*Penven et al.*, 2008].

2.2. Lagrangian Experiments With ARIANE

[10] The Lagrangian analyses are based on the offline mass-preserving algorithm ARIANE [*Blanke and Raynaud*, 1997; *Blanke et al.*, 1999; B. Blanke and N. Grima, Tutorial: First steps with ARIANE, sequential mode, 2008, http://www.univ-brest.fr/lpo/ariane], which is here used to calculate trajectories of numerical floats (particles) within the 2-day archive of a multiyear, three-dimensional velocity field. The approach allows the full description of individual trajectories as well as volume transport estimates based on the tiny weight allotted to each numerical float and transported without alteration along its trajectory. The volume of water transported from an initial to a final geographical section is computed by summing the transport of the numerical floats that achieve the connection that is being considered. Default information interpolated along individual trajectories includes salinity, temperature, depth, and density.

[11] All the Lagrangian experiments are conducted over the domain that spreads from 52°S to 25°S and from 8°W to 30°E. It is chosen smaller than the area covered by the ROMS simulation to avoid the inclusion of velocity data too close to the model open boundaries and possibly biased by the external SODA forcing. AAIW is characterized by a salinity minimum below the thermocline. Over the geographical sections where millions of particles were initialized (to account for an inward velocity), we kept only the particles associated with relevant salinity and density values, typical of this water mass. Each particle was associated with an individual weight related to the local magnitude of the incoming transport (expressed here in sverdrups per 2-day intervals; with 1 Sv = 10^6 m^3 s^{-1}). All particles were integrated forward in time until they reach one of the control sections (see section 4 for more details), with a maximum allowed integration time of 14 years to complete the connection (a negligible number of particles did not exit the control domain within this interval). The starting dates were taken sequentially from the first day of the fourth year of the model archive until the end of the sixth year. Conversely, for Lagrangian experiments run backward in time, the starting dates are taken during the last three years of the available archive. Insofar as the ocean model was run for twenty years, this sampling strategy did allow all the released particles to complete their integration within the 17-year subset of the archive suitable for analysis.

2.3. Characterization of Water Mass Dynamics

[12] The Agulhas retroflection region shows one of the strongest signals in kinetic energy within the world ocean. The multitude of submesoscale and mesoscale structures that circulate in the Cape Basin is an obvious sign of the turbulence that develops in the area. Mesoscale eddies and large Agulhas Rings, ejected from the Agulhas retroflection, are associated with the leakage of Indian Ocean water into the Atlantic basin [*Gordon*, 2003; *Richardson and Garzoli*, 2003]. The value of the Okubo-Weiss parameter (calculated from the zonal and meridional components of the flow) and the changes in the direction of the Lagrangian horizontal velocity of numerical particles are used to interpret the

dynamics of the water masses that converge in the Cape Basin.

2.3.1. Okubo-Weiss Parameter

[13] A criterion on the Okubo-Weiss parameter [*Okubo*, 1970; *Weiss*, 1991] is often used to diagnose coherent structures in specified flows. This parameter measures the relative dominance of strain and vorticity and is calculated as follows:

$$OW = \sigma^2 - \omega^2$$

where $\sigma = (\sigma_n^2 + \sigma_s^2)^{1/2}$ is the strain rate of the horizontal (u, v) velocity field, with its normal, $\sigma_n = \partial u/\partial x - \partial v/\partial y$, and shear, $\sigma_s = \partial u/\partial y + \partial v/\partial x$, components, and where $\omega = \partial v/\partial x - \partial u/\partial y$ is the vertical component of relative vorticity. For positive values of OW, the strain prevails, whereas negative values correspond to a dominant vorticity-based dynamics usually associated with vortex cores. This parameter can be used to characterize regions of concentrated vorticity, and thus of coherent eddies, in a given two-dimensional velocity field. For sake of simplicity, in this study, we only consider a nearest-neighbor interpolation of the Okubo-Weiss parameter (calculated on the model tracer grid points).

2.3.2. Directional Variations of Particle Trajectories

[14] The movement of a particle may be characterized by the change in the direction of its trajectory. For a given time index i and a given particle j, this direction (angle β) can be deduced by its successive 2-day displacements:

$$\alpha = \text{atan}\,(\Delta y/\Delta x)$$

where $\Delta x = x\,(j, i+1) - x\,(j, i)$ and $\Delta y = y\,(j, i+1) - y\,(j, i)$. The change in the direction of the particle's trajectory is then given by: $\beta\,(j, i) = \alpha\,(j, i) - \alpha\,(j, i-1)$. This winding-angle technique has certain similarities with the algorithm developed by *Sadarjoen and Post* [2000] and used by *Souza et al.* [2011] for detecting eddies with streamline geometry, but is built here on Lagrangian trajectories. A sequence of small values for $|\beta|$ (small curvature) is the sign that the particle is flowing within a jet or a filament whereas large values (large curvature) are likely associated with its capture by a coherent structure (meander or eddy), either cyclonic (for negative values of β) or anticyclonic. Yet, there is no straight way to define a priori the optimal threshold (β_0) that would separate conveniently the circulation within an eddy from the circulation within a filament. Therefore, the results will be presented as a continuous function of β_0 (see section 5.1).

3. Results from the Ocean Model

3.1. Comparison With Satellite Altimetry

[15] To evaluate the realism of our ROMS simulation, Figure 2 compares the model sea surface height with the absolute dynamic topography produced by Segment Sol Multimissions d'altimétrie, d'Orbitographie et de Localisation Précise/Data Unification and Altimeter Combination System (SSALTO/DUACS) [*Ducet et al.*, 2000].

[16] Monthly mean sea level fields are shown for January in Figures 2a and 2b for the observations (as an average over 2000–2007) and for the model (as an average over the last 16 years of simulation and gridded at the same horizontal resolution as the observations), respectively. The agreement between both maps is fair, even though the finer spatial scales allowed in the model and a blind zone in altimetry coverage near the coast lead to a cross-shore gradient along the southeastern coast of Africa more pronounced in the model. Notably, the eastward penetration of the Agulhas retroflection into the Atlantic Ocean is equivalent and the locations of the SAF (around 45°S at 0°E) and of the southern branch of the Subtropical Front (STF, around 36°S at 0°E) coincide. The geostrophic circulation deduced from the slopes of the sea surface is used to compute an eddy kinetic energy that is shown for January both for the observations (Figure 2c) and the simulation (Figure 2d). The modeled mesoscale eddy activity concentrates on the same oceanic regions as the observations, except with a slightly higher intensity. Contrastingly, satellite altimeter-derived eddy kinetic energy is somewhat greater than the modeled one in the region between the southwestward flowing Agulhas Current and the eastward flowing Agulhas Return Current: the vicinity of the eastern open boundary, where the model fields are forced to climatological values, is such as to damp a significant fraction of the model internal variability and can perturb locally the numerical solution.

3.2. AAIW Identification

[17] Figure 3 shows the AAIW salinity minimum, obtained after averaging the model results over the last 10 years of the simulation, together with its depth and local density values. We note first that the value of the salinity minimum increases northward and that four water types characterized by this minimum are present in the study area. In the southern part of the domain, the salinity minimum is within rather light and fresh surface waters ($1026.8 < \sigma_0 <$ l027.3 kg/m^3; $33.5 < S < 34.1$). These waters correspond to Subantarctic Surface Water (SASW) that flows south of the SAF [*Sievers and Nowlin*, 1984]. The salinity minimum in the western part of the domain, between 33°S and 45°S, corresponds to AAIW from the South Atlantic (A-AAIW) brought in the southeast Atlantic by the SAC. A-AAIW lies in the 600–1000 m layer north of 45°S, with salinity ranging between 34.2 and 34.5 and density between 1027.1 and 1027.3 kg/m^3. The meridional extent of this water mass decreases eastward. The AAIW that originates in the Indian Ocean (I-AAIW) joins the southeast Atlantic within the AC that flows along the African coast. At the level of the tip of South Africa, north of 42°S, the I-AAIW core is located mainly between 1000 and 1400 m depth, with salinity between 34.5 and 34.6 and density between 1027.3 and 1027.6 kg/m^3. North of 35°S, the southeastern Atlantic AAIW (SEA-AAIW) flows northwestward in the Benguela

Figure 2. Average January sea level for (a) the observations (as an average of AVISO/DUACS satellite altimetry over 2000–2007) and (b) the model (as an average over the last 16 years of simulation and gridded at the same 1/3° horizontal resolution as the observations), with a 10 cm contour interval. January eddy kinetic energy for (c) the observations and (d) the model, with a 0.05 m^2/s^2 contour interval.

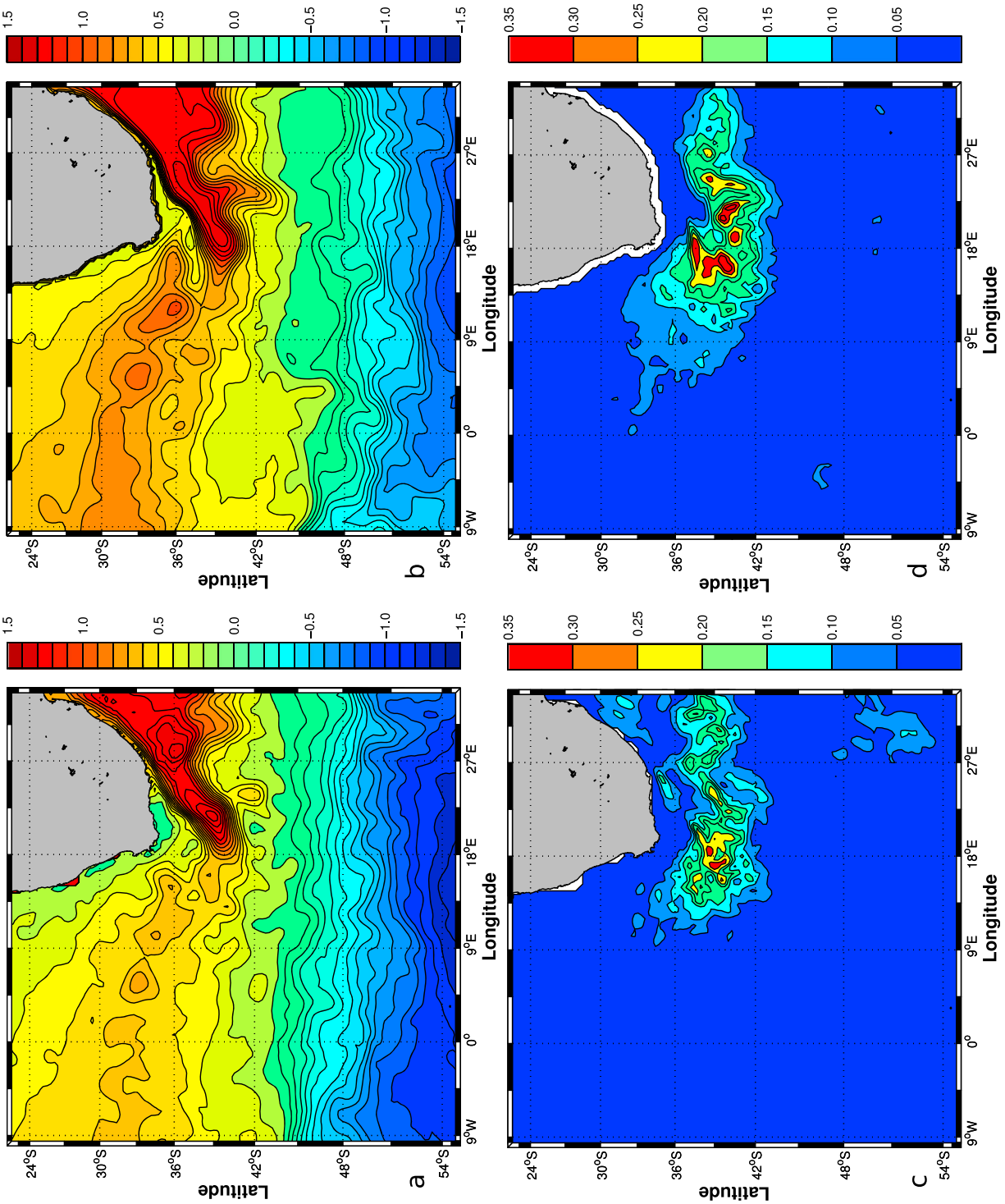
a
b
c
d
Latitude
Longitude
24°S
30°S
36°S
42°S
48°S
54°S
9°W
0°
9°E
18°E
27°E
1.5
1.0
0.5
0.0
−0.5
−1.0
−1.5
0.35
0.30
0.25
0.20
0.15
0.10
0.05

Figure 2

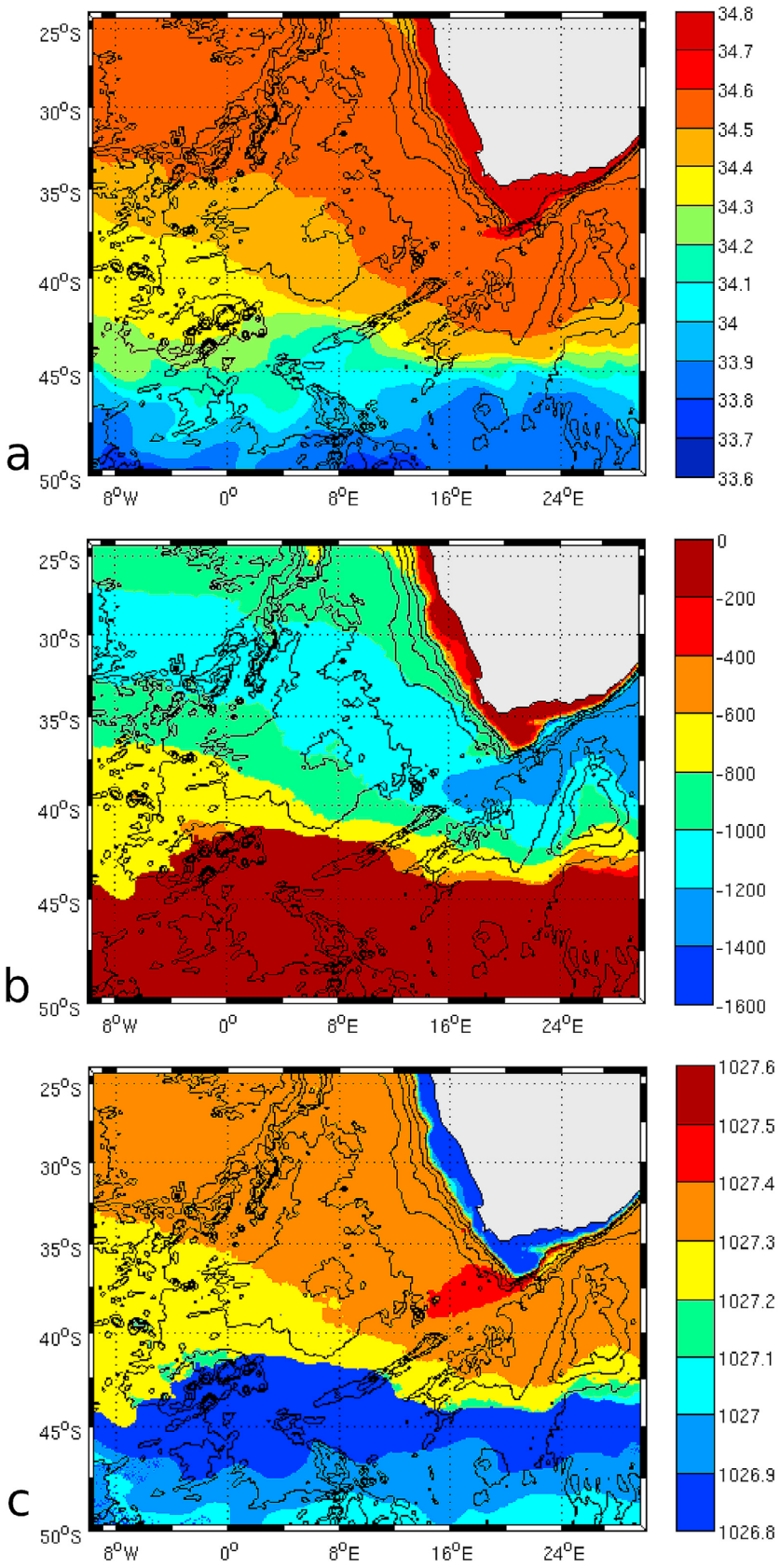

Figure 3. Maps of (a) the salinity minimum, (b) the depth of this minimum (in m), and (c) the value of the density at this depth (kg/m^3) calculated from the average of the last 10 years of simulation. Bathymetry is superimposed with contours drawn every 1000 m.

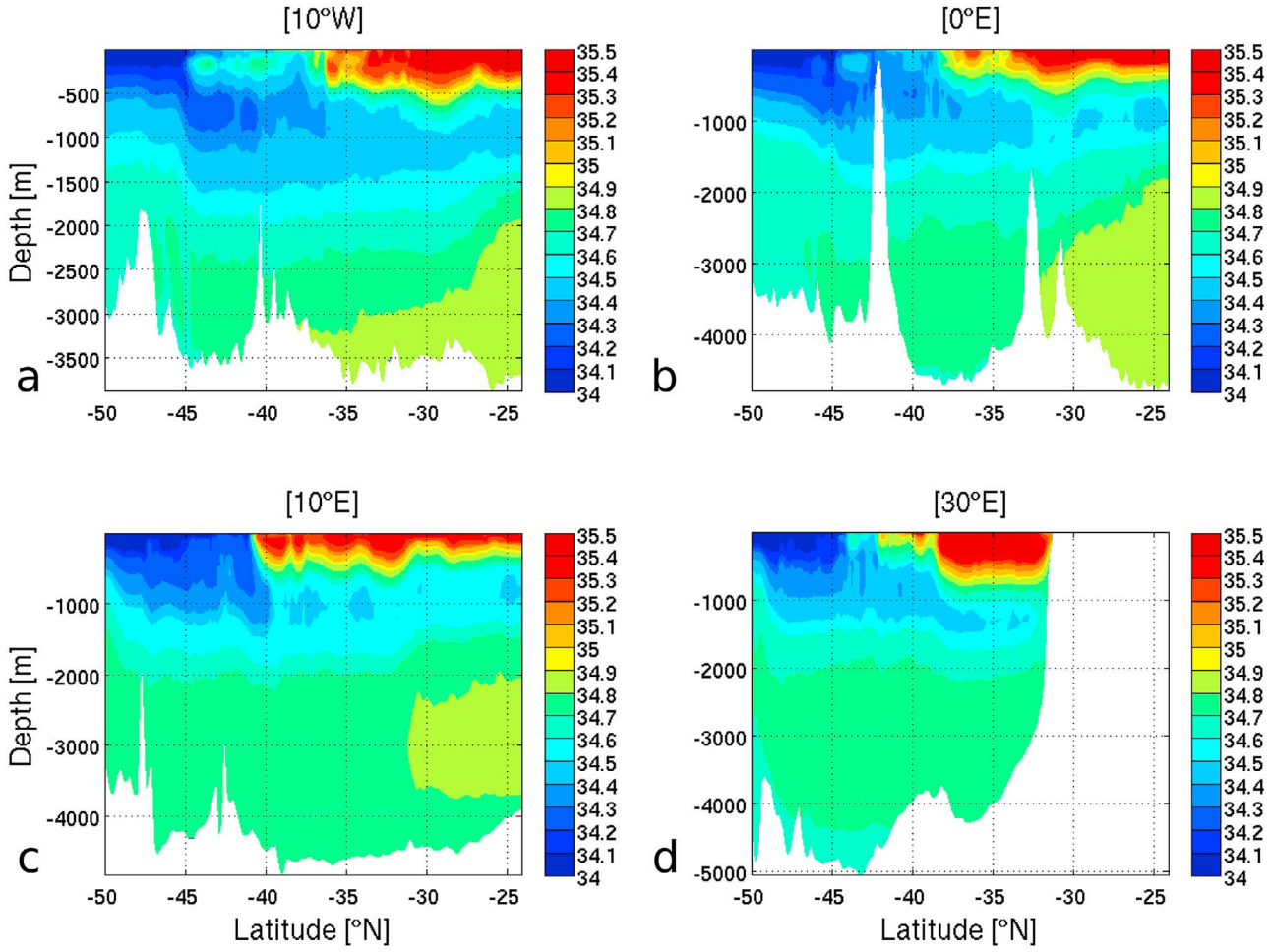

Figure 4. Model salinity sections between 24°S and 50°S on the first day of January (year 10) at (a) 10°W, (b) 0°E, (c) 10°E, and (d) 30°E.

Current. Downstream the Cape Basin, SEA-AAIW lies in the 600–1200 m layer with salinity varying between 34.5 and 34.6 and density between 1027.3 and 1027.4 kg/m^3.

[18] The four water masses characterized by a salinity minimum are easily spotted on meridional salinity sections drawn on Figure 4 on the first day of year 10 of the model simulation. South of 45°S, SASW spreads everywhere at the sea surface. From 45°S to 35°S, A-AAIW can be found at 10°W (Figure 4a) and 0°W (Figure 4b) with its core centered at 800 m depth and with salinity varying between 34.2 and 34.5. North of the section drawn at 30°E (Figure 4d), the core of I-AAIW is centered around 1200–1300 m depth with salinity between 34.5 and 34.6. The SEA-AAIW is visible at about 1000 m depth at 0°E and 10°E, between 30°S and 25°S, with salinity in the range 34.5−34.6. It is worth noting that these AAIW varieties are very difficult to spot southwest of Africa at 10°E (between 40°S and 30°S, Figure 4c). This area corresponds geographically to the Cape Basin and is characterized by very turbulent dynamics [*Boebel et al.*, 2003].

[19] Alternatively, these water masses can be identified in potential temperature versus salinity diagrams drawn the same day of the model simulation (Figure 5). At 10°W and 30°E, SASW is identified as a surface salinity minimum at high latitudes (south of 45°S). At 10°W (Figure 5a), i.e., in the Atlantic Ocean, the salinity minimum below the thermocline is less than 34.5 south of 34°S, and corresponds to A-AAIW. North of 34°S, SEA-AAIW can be found with a salinity minimum between 34.5 and 34.6. At 30°E (Figure 5b), i.e., in the Indian Ocean, I-AAIW is identifiable by a salinity minimum mainly between 34.5 and 34.6. The density anomalies associated with these salinity minima range from 27.0 to 27.4 kg/m^3. They are closer to 27.2 kg/m^3 for A-AAIW, and closer to 27.3 kg/m^3 for I-AAIW and SEA-AAIW.

[20] Table 1 shows that A-AAIW and I-AAIW are hence differentiable in the simulation by their salinity minimum and their depth (closely related to their density). The A-AAIW core found at 10°W between 46°S and 34°S and from 600 to 1000 m depth has salinity ranging from 34.2 to 34.5, whereas the I-AAIW core found at 30°E in the AC lies between 1000 and 1400 m within the 34.5−34.6 salinity range. Therefore, A-AAIW is fresher, shallower and lighter than I-AAIW and, according to the model, 34.5 is the salinity limit that differentiates best the Indian and Atlantic origins of the AAIW found in the southeast Atlantic.

3.3. Validation of the Model Salinity and Density Fields

[21] We compare here the results of the regional model with in situ observations provided by the Argo profiling

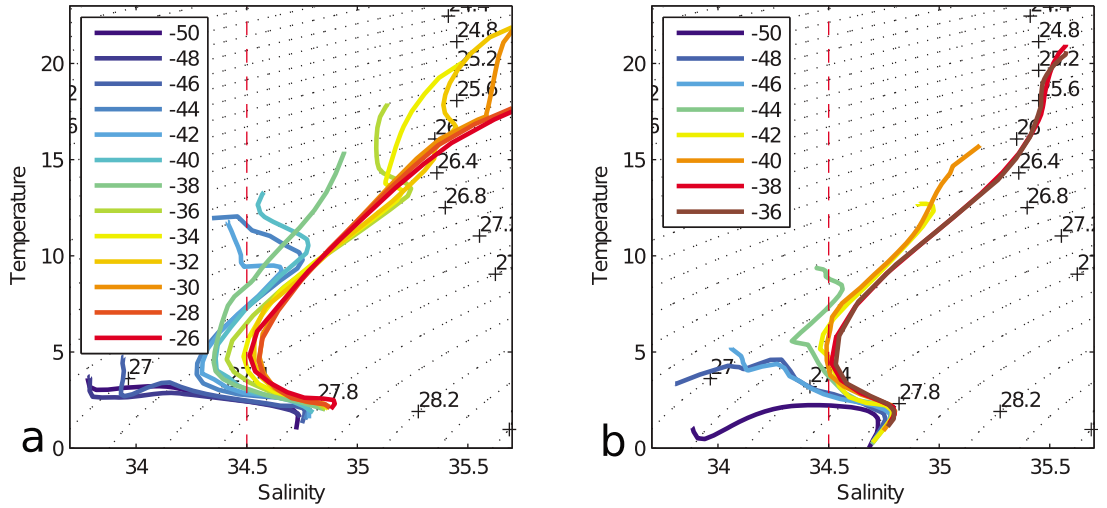

Figure 5. Model Θ-S diagrams (temperature in [°C]) between 26°S and 50°S on the first day of January (year 10) at (a) 10°W and (b) 30°E. Salinity 34.5 is drawn in red. Isopycnals (expressed in σ_0 units) are superimposed with dotted lines with a 0.2 interval.

floats drifting around Southern Africa between 2004 and 2010 [*Speich et al.*, 2012; E. Rusciano et al., submitted manuscript, 2012], with near-bottom CTD casts done at 80 stations in February–March 2008 during the BONUS-GoodHope cruise (E. Rusciano et al., submitted manuscript, 2012), and with a collection of historical samples and modern data [*You et al.*, 2003]. Two AAIW varieties can be found in the salinity and density meridional sections derived from the BONUS-GoodHope cruise and from the model: A-AAIW and I-AAIW (E. Rusciano et al., submitted manuscript, 2012).

[22] From a qualitative point of view, the structures in salinity minimum derived from Argo floats data, selected sea experiments and the model simulation (Figure 3) look alike. The salinity minimum shows higher values in the AC than in the southwest of the studied domain (note that the maps in Figures 3a and 3c in *You et al.* [2003] are calculated on the 1027.4 kg/m^3 isopycnal surface). From a quantitative point of view, the maps obtained by *You et al.* [2003] and *Speich et al.* [2012] are similar, but they differ from the numerical results of the simulation. According to *Speich et al.* [2012], I-AAIW can be identified north of the SAF by salinity values greater than 34.3, whereas the waters that are freshly ventilated in the Southern Ocean, south of the STF and north of the SAF, are characterized by salinity values lower than 34.3. According to *You et al.* [2003], the salinity minimum varies from 34.1 to 34.3 in the southwest of the domain, and from 34.4 to 34.7 in the AC. Therefore, salinity along the 1027.4 kg/m^3 isopycnal surface is lower than 34.3 in the Atlantic and greater than 34.4 in the Indian Ocean.

[23] Our numerical results show that this salinity minimum varies from 34.5 to 34.6 in the South West Indian Ocean and from 34.2 to 34.5 in the South Atlantic. Therefore, the model overestimates the salinity minimum by 0.2 with reference to in situ measurements. This is why, in the simulation, 34.5 is the salinity that differentiates at best I-AAIW and A-AAIW, though the threshold deduced from in situ measurements is rather 34.3 [*You et al.*, 2003; *Speich et al.*, 2012; E. Rusciano et al., submitted manuscript, 2012]. In the same way, SEA-AAIW shows salinity ranging from 34.55 to 34.6 in the simulation, whereas the range obtained by *You et al.* [2003] and *Speich et al.* [2012] is 34.3−34.5.

[24] In their potential temperature versus salinity diagram, *You et al.* [2003, Figure 4a] showed that I-AAIW is saltier than 34.3 and that dAAIW, which corresponds to A-AAIW, has salinity ranging from 34.1 to 34.3. South of Africa, the AAIW salinity minimum and associated temperature range from 34.153 to 34.559 and 3.31°C to 6.15°C, respectively [*Jacobs and Georgi*, 1977]. Equivalent values have been observed during the BONUS-GoodHope cruise (i.e., southwest of Africa, between 0°E and 14°E and south of 34°S): the in situ data show a salinity minimum below the thermocline ranging from 34.15 to 34.46 [*Arhan et al.*, 2011; E. Rusciano et al., submitted manuscript, 2012]. The Θ-S diagrams confirm a 0.2 overestimation of the salinity minimum by the model because the salinity minimum varies from 34.2 to 34.5 and from 34.5 to 34.6, in the South Atlantic and in the South West Indian Ocean, respectively (Figure 5). Despite this bias, CTD casts and model results agree in positioning AAIW north of 46°S.

[25] The horizontal depth patterns of the salinity minimum also agree between the model and in situ observations. In *You et al.* [2003], the AAIW core, calculated on the 1027.4 kg/m^3 isopycnal surface, is at an average depth of 900 m in the South Atlantic and at an average depth of 1200 m in the Indian Ocean. According to E. Rusciano et al. (submitted manuscript, 2012), AAIW flows at depths between 600 and

Table 1. Ranges for Salinity, Depth and Density Anomaly (σ_0, Referenced to 0 dbar) Corresponding to the Salinity Minimum for 3 Specific Water Masses Within the Model Domain

Water Mass	SASW	A-AAIW	I-AAIW	SEA-IAAIW
Salinity	33.6−34.1	34.2−34.5	34.5−34.6	34.5−34.6
Depth (m)	0−200	600−1000	1000−1400	800−1200
σ_0 (kg/m^3)	<27.1	27.1−27.3	27.3−24.6	27.3−27.4

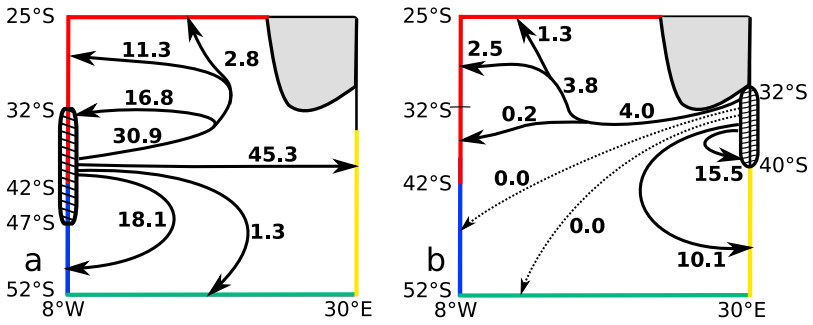

Figure 6. Control sections for the Lagrangian experiments (colored segments) and mass transfer estimates for (a) A-AAIW and (b) I-AAIW. The hatched areas at 8°W and 30°E correspond to the initial sections used in the experiments run forward in time. Bold figures give in sverdrups the mass transfers for waters with initial salinity and density in the ranges 33.9−34.7 and 1027.1−1027.6 kg/m^3, respectively.

1000 m in the South Atlantic Ocean and from 800 to 1400 m in the Indian Ocean. In situ values from these two data sets are similar, although the 1027.4 kg/m^3 isopycnal surface is deeper than the salinity minimum in the South Atlantic and shallower in the South West Indian Ocean. Therefore, the A-AAIW and I-AAIW cores flow at the right depths in the simulation. Observational data and model results show that the A-AAIW layer is shallower than the I-AAIW layer.

4. Lagrangian Results

4.1. AAIW Pathways and Transformation

[26] Several Lagrangian experiments were conducted to characterize the modeled AAIW varieties that converge in the Benguela Current. As explained in section 2.2, the individual weights of the particles are summed according to their final interception section in order to derive directional transports [*Blanke and Raynaud*, 1997]. The geometry of the transfers is diagnosed following *Blanke et al.* [1999], by recording the passage of each particle and summing algebraically its transport at each velocity point of the three-dimensional grid, before vertical integration and derivation of a Lagrangian stream function. Figure 6 shows the control sections used for the Lagrangian experiments and the volume transports diagnosed between these sections. A preliminary experiment is run backward in time from the north-northwest (NNW) of the domain (i.e., the western section at 8°W from 42°S to 25°S, and the northern section at 25°S from 8°W to the African continent; red line in Figures 6a and 6b) to specify, in the model, appropriate physical property ranges for intermediate waters, which may somewhat differ from observational values. In the following, the combination of these two sections will be called the north-northwest (NNW) section. Initial positions for the numerical particles are spread over the last 3 years of the available model archive and integrated backward in time for a maximum duration of 14 years. This approach allows the definition of suitable entry windows for AAIW in the Indian Ocean and in the South Atlantic by analyzing the origins of the particles close to the subthermocline salinity minimum on the NNW section: the AAIW that reaches the northwestern area of our domain comes from the South Atlantic (at 8°W) between 47°S and 32°S and from the Indian Ocean (at 30°E) between 40°S and Africa (at 32°S). The physical properties that describe at best the modeled AAIW at these sections are the ranges 33.9 to 34.7 and 1027.0 to 1027.6 kg/m^3, for salinity and density, respectively. Using now these definitions as initial windows for forward Lagrangian integrations, we can track AAIW particles that enter the domain either eastward at 8°W or westward at 30°E.

[27] We find that the I-AAIW can retroflect eastward, within the return branch of the AC north of 40°S (15.5 Sv) or further south (10.1 Sv). An insignificant fraction of I-AAIW makes it way to 8°W south of 42°S, and the export to the Atlantic Ocean is intercepted by the NNW section (4.0 Sv, out of which 3.8 Sv end north of 32°S). The A-AAIW that originates in the South Atlantic is partly transmitted eastward to the Indian Ocean as part of the ACC (45.3 Sv). The rest either recirculates westward south of 42°S (18.1 Sv) or reaches the NNW section (30.9 Sv, out of which 14.1 Sv end north of 32°S). Only a small fraction of A-AAIW flows south of 50°S (1.3 Sv). It is worth noting that on this Atlantic side the entry and exit windows overlap (from 42°S to 32°S). Therefore, a significant fraction of the transfer diagnosed north of 42°S is likely associated with short forward and backward movements around 8°W, possibly within mesoscale structures.

[28] We can filter out roughly this transfer by imposing two additional conditions on the trajectories: first a minimum residence time within the domain of integration (4 months), second a net northward displacement between the initial and final positions at 8°W. With these additional assumptions, the transfer north of 42°S falls to 18.3 Sv, with still 13.7 Sv transmitted north of 32°N. Therefore, the large-scale northward transfer of A-AAIW from the latitude band 47°S–32°S to the band 42°–32°S is estimated at 4.6 Sv.

[29] In-depth investigation of the behavior of each AAIW variety asks for the detailed analysis of the full set of trajectories that define each transfer. From now on, to characterize better each variety and also reduce the computational cost of the processing, we adopt a definition that emphasizes the contrast of both AAIW varieties at their origins. We refine the density range to 1027.1–1027.55 kg/m^3 and we restrict the initial salinity to the range 34.2–34.5 (34.5–34.6) for A-AAIW (I-AAIW) at 8°W (30°E). With these new definitions, related to the core of the AAIW layer, the transfers of A-AAIW and I-AAIW to the NNW section amount to 11.7 and 2.4 Sv, respectively (instead of 18.3 and

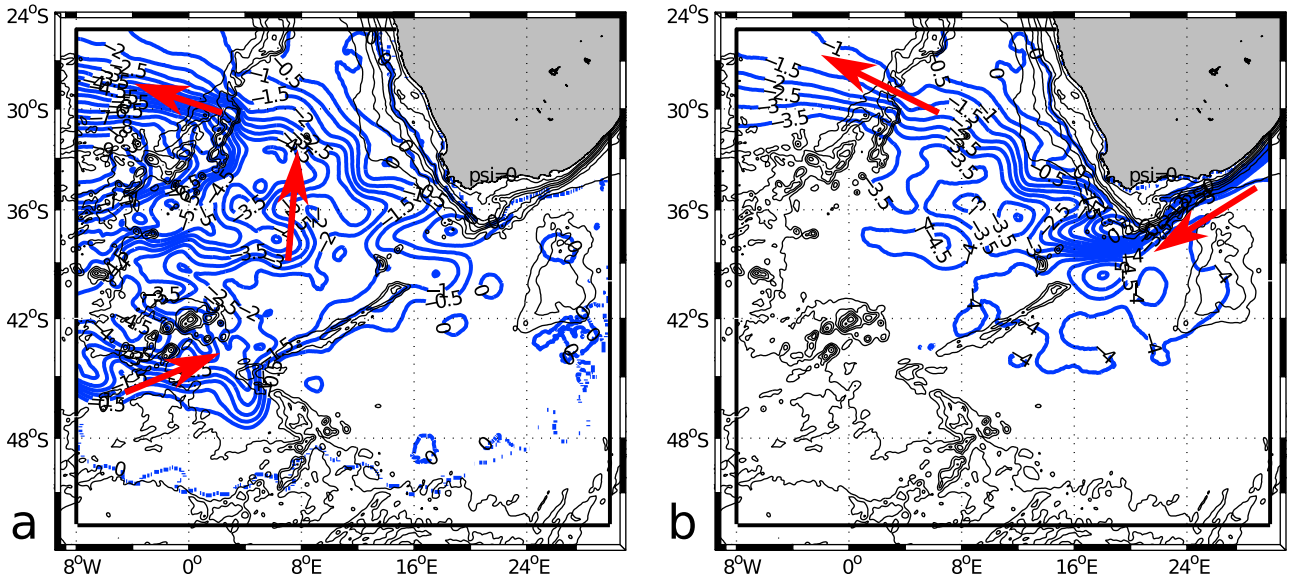

Figure 7. Lagrangian stream function for the transfer of AAIW to the north-northwest section for NA-AAIW from 8°W within the salinity range 34.2–34.5 (a) and for I-AAIW from 30°E within the salinity range 34.5–34.6 (b). The contour interval is 0.5 Sv and the value of the stream function is arbitrarily set to 0 over Africa.

4.0 Sv previously). Following the method introduced by *Blanke et al.* [1999], the pathways followed by these transfers are shown in Figure 7, with a 0.5 Sv contour interval.

4.1.1. A-AAIW Pathways and Evolution

[30] A-AAIW pathways are complex because there are multiple entry windows at 8°W, especially at 46°S within the SAF and at 35°S within the STF. The flow narrows at several key locations closely associated with topographic barriers and ridges. Therefore, the following discussion will distinguish two branches of A-AAIW. We designate the first one as Southern A-AAIW (SA-AAIW). It encompasses the A-AAIW particles that do not cross the imaginary line from (8°W, 34°S) to (16°E, 48°S) (Figure 8). Hence, these particles recirculate to 8°W (between 34°S and 42°S) after only a small spread in the domain. The second one, which we designate as Northern A-AAIW (NA-AAIW), includes all the other A-AAIW particles. These particles end up circulating in the same horizontal domain as the particles associated with I-AAIW. The differentiation between SA-AAIW and NA-AAIW is made possible by the knowledge of the trajectory details of the particles that participate in each transfer. Our experiments suggest that the transport of the southern and northern varieties of A-AAIW to the NNW section amount to 1.8 and 9.9 Sv, respectively.

[31] Figure 8 shows that the penetration of SA-AAIW (1.8 Sv) in the domain is rapidly blocked by broad and steep bottom topography: the Discovery Seamounts to the east, and the RSA Seamounts to the north. As a consequence, SA-AAIW recirculates rapidly to 8°W south of 33°S, mostly in the 44°S – 39°S latitude band, without making its way to the Cape Basin. During its journey, it remains within the 600–1000 m depth and 34.2–34.5 salinity ranges. Altogether, the salinity of the SA-AAIW branch increases only by +0.07 (Table 2) during its journey in the domain. These salinity gains take place mostly above topographic features.

[32] NA-AAIW (9.9 Sv) enters the domain within the eastward-flowing SAC. It bends northward and crosses the Cape Basin before flowing westward over the Walvis Ridge (Figure 7a). At its origin at 8°W, this water mass flows between from 800 and 1000 m depth and has salinity between 34.2 and 34.5. In the Cape Basin, it deepens (down to 1200 m) and its salinity increases abruptly. Salinity increases again over the Walvis Ridge where it reaches the

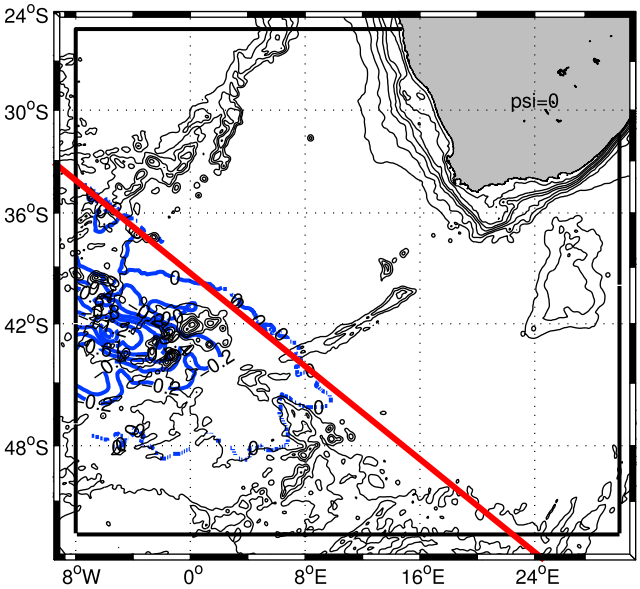

Figure 8. Lagrangian stream function for the transfer of SA-AAIW from 8°W to the north-northwest section. The contour interval is 0.2 Sv and the value of the stream function (in blue) is arbitrarily set to 0 over Africa. The red line is the imaginary line from (8°W, 34°S) to (16°E, 48°S) that the A-AAIW particles do not cross.

Table 2. Average Depth and Salinity of the Three AAIW Varieties Identified in the Simulation[a]

	A-AAIW		
	NA-AAIW	SA-AAIW	I-AAIW
Initial depth (m)	−885 (231)	−893 (263)	−1198 (242)
Final depth (m)	−1015 (273)	−962 (305)	−924 (295)
Net upward displacement (m)	−130	−69	+274
Initial salinity	34.38 (0.07)	34.36 (0.07)	34.60 (0.04)
Final salinity	34.58 (0.05)	34.43 (0.07)	34.60 (0.09)
Net salinity gain	+0.20	+0.07	0

[a]SA-AAIW escapes westward before reaching the Cape Basin, whereas NA-AAIW and I-AAIW flow to the northwest of the domain after they cross the Cape Basin. Associated standard deviations are given in parentheses.

range 34.55 – 34.6. Ultimately, at the NNW section, the net gain in salinity is +0.20 (Table 2).

[33] To visualize better the change in physical properties experienced by NA-AAIW, we analyzed the detailed displacements of a few particles. For each particle we compare the joint evolution of salinity, depth, and the Okubo-Weiss parameter (Figure 9). Though they follow rather distinct pathways, they all correspond to a salinity and depth increase between their initial and final states. The first one is the freshest particle initialized at 8°W in the NA-AAIW vein (Figure 9a); it underlines conveniently the salinity and depth increase experienced across the domain. The second one is the slowest to get to the NNW section (Figure 9b); it is captured by several coherent structures and illustrates the links between salinity variations, vertical displacements and small-scale dynamics. For the first particle, the net gain in salinity (+0.40) corresponds to a strong salinity and depth increase at the crossing of a highly turbulent area associated with large variability in the Okubo-Weiss parameter. Contrastingly, the slowest particle experiences successive salinity gains and losses with many upward and downward displacements along its journey, again with concomitant variations of the Okubo-Weiss parameter. The net salinity gain diagnosed along the full trajectory is +0.26. For both particles, the net gain in salinity is larger than the local salinity changes that can be related to changing values of the Okubo-Weiss parameter. It is worth noting here that the Okubo-Weiss parameter only reveals Eulerian coherent structures, and is mostly useful to detect strong eddy cores in a frozen velocity field. New techniques based on the concept

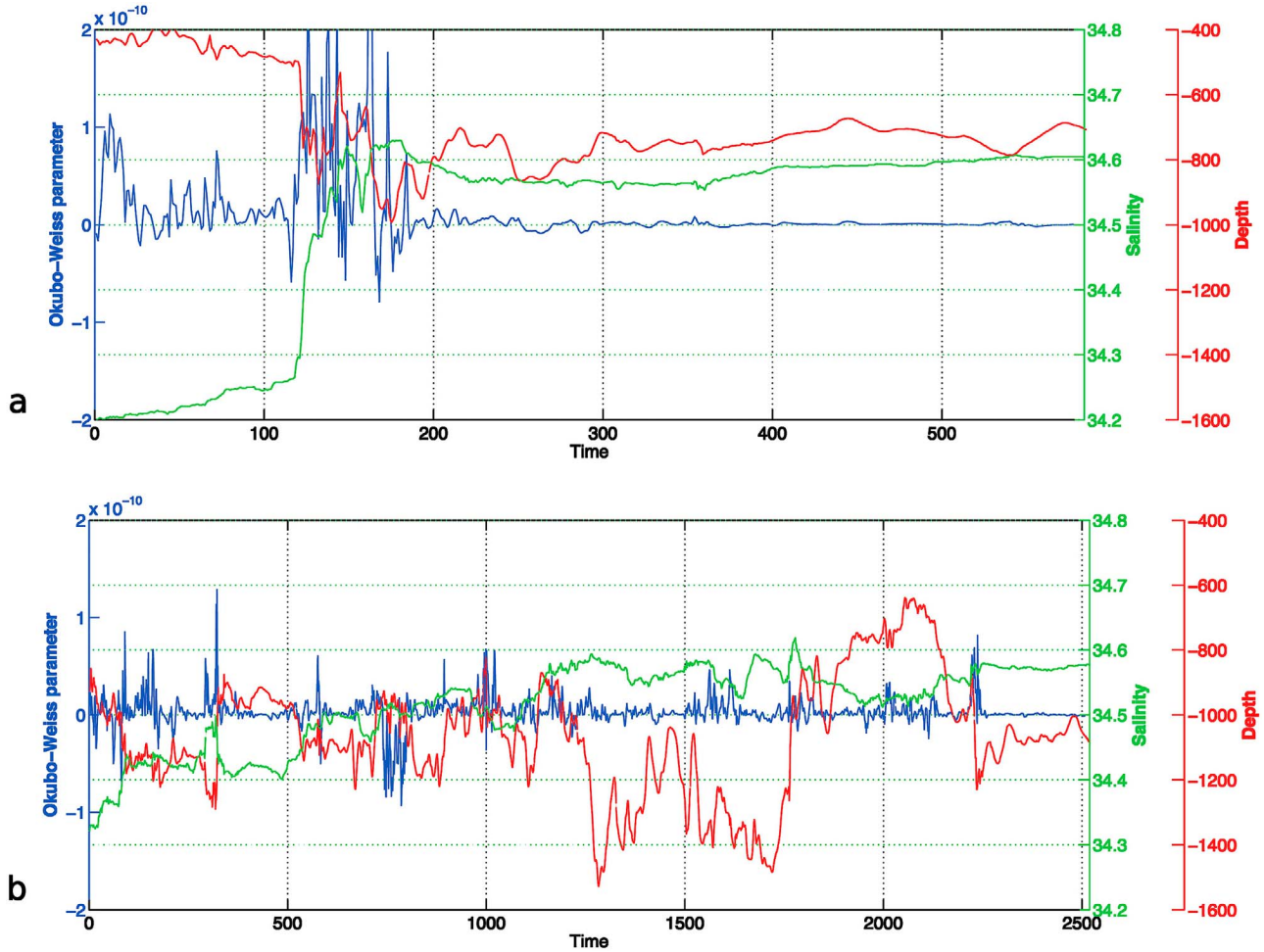

Figure 9. Time evolution of the Okubo-Weiss parameter (blue curve, in s^{-2}), salinity (green curve) and depth (red curve, in m) along the trajectories of (a) the freshest and (b) the slowest particles initialized at 8°W and part of the NA-AAIW transfer. Time is expressed as 2-day periods.

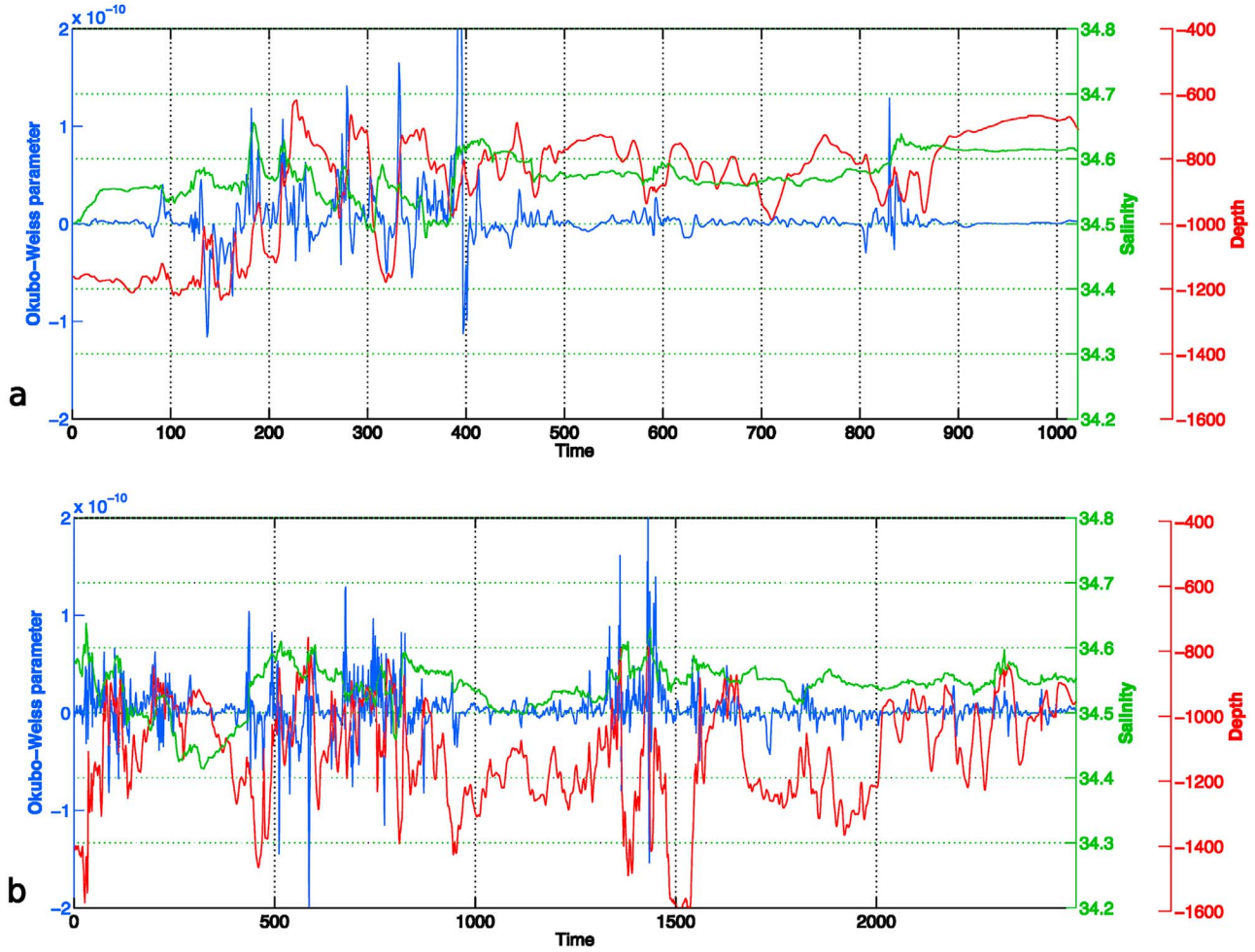

Figure 10. Time evolution of the Okubo-Weiss parameter (blue curve, in s^{-2}), salinity (green curve) and depth (red curve, in m) along the trajectories of (a) the freshest and (b) the slowest particles initialized at 30°E and part of the I-AAIW transfer. Time is expressed as 2-day periods.

of Lagrangian coherent structures [e.g., *d'Ovidio et al.*, 2004; *Beron-Vera et al.*, 2008] prove powerful to extract Lagrangian fields from oceanic mesoscale flows, but were not used in this study.

4.1.2. I-AAIW Pathways and Evolution

[34] The I-AAIW transfer (2.4 Sv) to the NNW section is strongly constrained by topography along the continental slope of southeastern Africa where I-AAIW flows smoothly within the AC till it reaches the southern limit of the Agulhas Bank (Figure 7b). It enters the Atlantic basin within the Agulhas Current System. Beyond that point, it crosses northwestward the Cape Basin, before flowing over the Walvis Ridge and continuing its journey westward. The integrated vision, both in time and in depth, shows first an eastward then a westward movement within the Cape Basin, along the northwestward transfer of I-AAIW to the Atlantic. Both an anticyclonic cell and a cyclonic cell edge the inflow in the Cape Basin. The first cell is associated with the retroflection of the AC. The second cell corresponds to the integrated effect of Agulhas Bank cyclones that are generated along the southwestern edge of the Agulhas Bank [*Penven et al.*, 2001; *Boebel et al.*, 2003; *Lutjeharms et al.*, 2003]. At 30°E in the Indian Ocean, I-AAIW flows within depths from 1000 to 1400 m. Slightly before entering the Cape Basin, it upwells and stabilizes at 800 to 1200 m depth. Along its journey, its signature in salinity does not depart from its initial range at 30°E (from 34.5 to 34.6), except for a small decrease in the Cape Basin and a small increase along the Agulhas Bank and over the Walvis Ridge. There is no net gain or loss in salinity (Table 2) and the salinity range on the final interception section is 34.55 – 34.60.

[35] To visualize better the changes in physical properties experienced by the I-AAIW, we present also for this water mass the detailed displacements of some particles (Figure 10). For the first particle that corresponds to the freshest particle initialized at 30°E, the net gain in salinity is 0.11 and the net upward displacement is about 500 m (Figure 10a). However, local variations along the trajectory can be as large as 0.18 for salinity and 600 m for depth. The second trajectory corresponds to the slowest particle of the transfer (Figure 10b). The net gain in salinity is −0.02, with local changes up to 0.22. The net upward displacement is about 400 m with local changes up to 800 m. Therefore, the net variation in depth and salinity for I-AAIW could be smaller than local variations (decreases and increases) and the full Lagrangian tracking of this water mass brings more

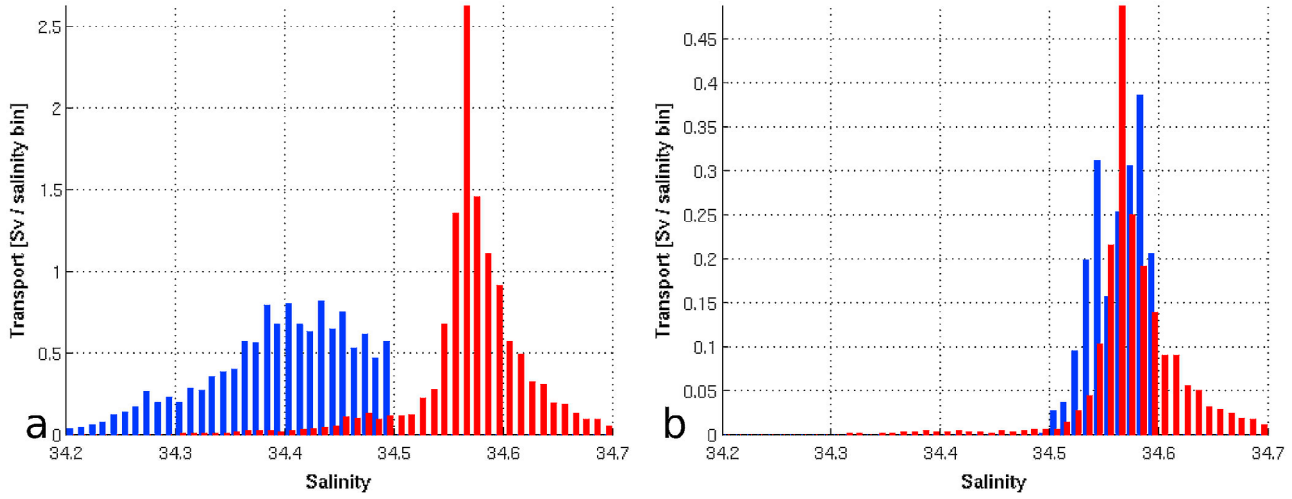

Figure 11. Transport (Sv per salinity bin) histogram as a function of initial (in blue) and final (red) salinity with 0.01 bins, for the (a) NA-AAIW and (b) I-AAIW transfers.

information than the mere comparison of statistics for the initial and final properties. For both particles, changes in physical properties are again related to changes in the value of the Okubo-Weiss parameter.

[36] Salinity and depth variations combine with strong variability in the Okubo-Weiss parameter diagnosed along the trajectories. This is an indication that the stirring induced by the interaction of mesoscale eddies and frontal areas is responsible for a significant fraction of the along-trajectory tracer variations.

[37] The Atlantic variety of AAIW (A-AAIW) splits into two branches. A northern one, NA-AAIW, experiences large increases in salinity and depth at the entrance of the Cape Basin. A southern one, SA-AAIW, has its eastward progression blocked by the Discovery Seamounts and recirculates back to 8°W mostly south of 34°S with little alteration of its salinity. The Indian variety of AAIW (I-AAIW) upwells slightly in the water column but without net alteration of its salinity during its eastward journey, despite strong local variations. The Lagrangian tracking of the main physical properties shows that local variations along a given trajectory can exceed largely the net change diagnosed between the initial (at 8°W or at 30°E) and final (on the NNW section) states. Such strong variations in salinity and depth combine with dynamical events that can be identified with the Okubo-Weiss parameter.

4.2. NA-AAIW and I-AAIW Physical Properties Changes

[38] NA-AAIW and I-AAIW experience contrasted changes in salinity and depth on their journey to the southeast Atlantic, as shown by the histograms of transport binned as a function of these quantities at the initial and final control sections (Figure 11). The salinity ranges for NA-AAIW and I-AAIW at their initial sections are by construction 34.2–34.5 and 34.5–34.6, respectively. However, when they exit the Cape Basin, both AAIW varieties show equivalent salinity values, ranging from 34.55 to 34.6. More precisely, the peak of the outflow is made of particles with final salinity between 34.56 and 34.57 for both origins. The histograms of the transfer binned as a function of initial and final salinity superimpose easily for I-AAIW, whereas they are well separated for NA-AAIW, which expresses the significant salinity increase experienced by the latter water mass during its journey. The histograms of transport binned as a function of initial and final depth in Figure 12 show that NA-AAIW and I-AAIW converge to the same depth range (from 700 to 1100 m), yet originating from contrasted depths: 600 to 1000 m and 1000 to 1400 m, respectively.

[39] We can estimate quantitatively the property variations experienced by the two AAIW varieties by mapping horizontally the gains and losses of salinity along the trajectories of the particles that participate in each connection (Figure 13). For this calculation, the salinity changes are diagnosed between successive positions (archived every 2 days) and remapped on a regular $1^\circ \times 1^\circ$ grid by summing algebraically the individual and local salinity changes weighted by the transports allotted to the corresponding particles. The spatial integration of this field is roughly equal to the magnitude of the transfer multiplied by the mean difference in salinity between the final and initial sections. Three regions stand out as preferential areas for altering the I-AAIW salinity (Figure 13b). The edge of the Agulhas Bank and the region over the Walvis Ridge are associated with significant salinity increase, whereas the southwest portion of the Cape Basin shows salinity losses. In the case of NA-AAIW (Figure 13a), only salinity gains show through the analysis. The gains in salinity are especially pronounced over the Discovery Seamounts, over the Walvis Ridge, and in the southwest portion of the Cape Basin. Indeed, NA-AAIW and I-AAIW converge in that specific region, with NA-AAIW being the freshest of the two AAIW varieties and the freshest water present in the whole water column. Interaction with neighboring water masses can only increase the salinity of NA-AAIW. Conversely, I-AAIW gets fresher on contact with NA-AAIW in the Cape Basin where they can mix efficiently. Over topographic features such as the continental slope of the Agulhas Bank or the Walvis Ridge, I-AAIW and NA-AAIW are forced to upwell in the water column and mix the saltier waters of the permanent thermocline.

[40] Further investigation is needed to address the I-AAIW increase in salt content when it flows along the Agulhas

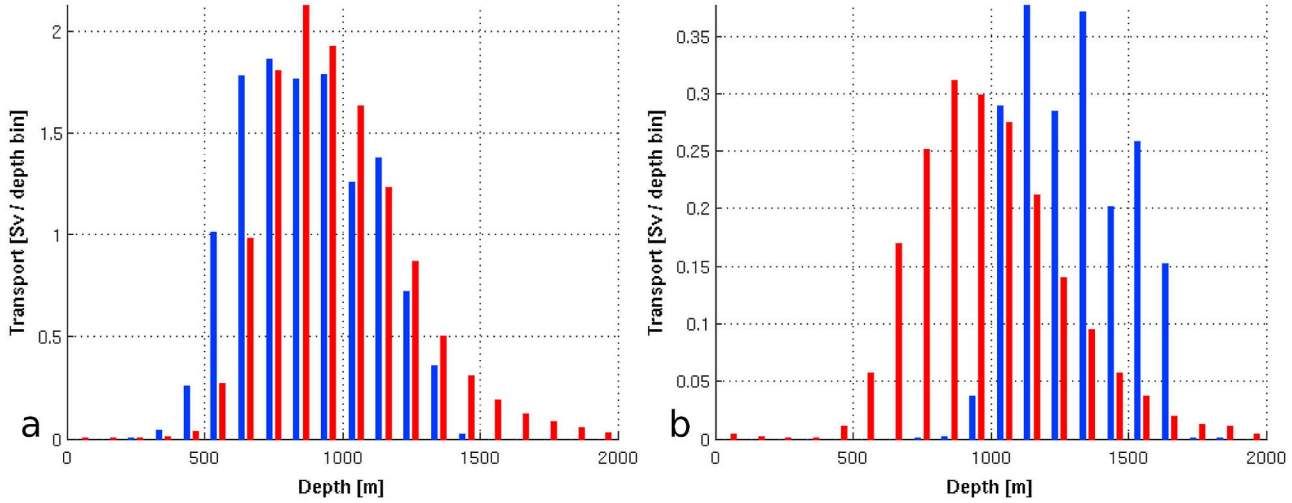

Figure 12. Transport (Sv per depth bin) histogram as a function of initial (in blue) and final (red) depth with 100 m bins, for the (a) NA-AAIW and (b) I-AAIW transfers.

Bank. This process develops mostly in regions where the continental slope is locally less steep (i.e., at 22°E and 26°E) and where the alongshore flow is thus subject to local acceleration or deceleration [*Speich et al.*, 2006]. However, a careful study of the vertical velocities and turbulent diffusion coefficients calculated by ROMS did not allow an unambiguous explanation of the physical mechanisms at play. A local and thorough comparison of the results obtained with the two available model archive rates (every 2 days or every 4 h) allows asserting that the Lagrangian analysis is not modified by a higher temporal resolution of the velocity output and that the increase in salt content is not related to some faulty strategy in the archive of the model fields.

4.3. NA-AAIW and I-AAIW Dynamical Behavior

[41] Insofar as a geometrical criterion can prove successful in detecting eddies [see, e.g., *Souza et al.*, 2011], we supplement the diagnosis of the Okubo-Weiss parameter with a more robust approach, based on the variation of direction of the trajectory of all the numerical particles that participate in the NA-AAIW and I-AAIW transfers. The analysis is conducted in four separate zones delimited in Figure 13: Zone 1-I [21°E–29°E] × [33°S–38°S] corresponds to the area where I-AAIW is transported by the AC; Zone 1-A [8°W–3°E] × [34°S–46.5°S] is the exit region from the SAC for NA-AAIW; for both water masses, Zone 2 [5°E–20°E] × [33°S–42°S] is associated with northward deflection and crossing of the Cape Basin; Zone 3 [0°E–5°E] × [26°S–33°S] corresponds to flow over the Walvis Ridge.

[42] For each particle, we calculate the histogram of the changes of direction of each particle trajectory (i.e., the angle β, see section 2.3) between successive displacements evaluated every two days. In each zone, the individual histograms are combined into a single cumulative histogram with a weighting system based on the transport allotted to each particle present in the area. This histogram is interpreted in the light of its proportion lying above (or below) an unspecified threshold β_0. Figure 14 shows an example for both the cumulative histogram, where a specific value of β_0 is used to separate different dynamics, and the relative importance of these dynamics according to the evolution of β_0: anticyclones (percentage A), cyclones (percentage C), eddies (A + C) and filaments (100-A-C). Indeed, there is no straight way to define the optimal threshold that would distinguish at best the movements in an eddy and the movements in a filament. As opposed to that, it is still possible to compare the behavior of distinct water masses, possibly in different zones, by comparing the proportion of each histogram lying between $-\pi$ and $-\beta_0$ (cyclonic-like movement), between $-\beta_0$ and $+\beta_0$ (filaments) and between $+\beta_0$ and $+\pi$ (anticyclonic-like movement), for any arbitrary choice of β_0. Meaningful values for β_0 might be deduced from the typical rotation frequency of the mesoscale eddies found in the Cape Basin. Using typical eddy radius and tangential velocity observations from *Arhan et al.* [2011] (70 km and 15 cm/s), the rotation angle over a two-day interval is equal to 21 degrees.

[43] The analysis was done first for the full length of the trajectories, regardless of possible recirculation loops, and second by considering only the first passage in each zone. In Zone 2, the propensity of I-AAIW to flow within eddies, and notably within cyclones, is sharpened when only the first passage is taken into account. Similarly, in Zones 1-A and 2, the tendency of NA-AAIW to flow within filaments is sharpened when only the first passage is taken into account. Indeed, considering all the passages through a given zone tends to smooth out the differences that may exist between various dynamics. For a given particle, the first passage can be used to characterize the original dynamics of the water mass being tracked, whereas subsequent re-entries may correspond to already modified physical properties. In order to concentrate on the original properties of each water mass, we will discuss only the results obtained for the first passage of the particles in each zone.

[44] I-AAIW enters the Atlantic Ocean within the AC (Zone 1-I) and this stage corresponds to the largest proportion of circulation within a filament-like dynamics found

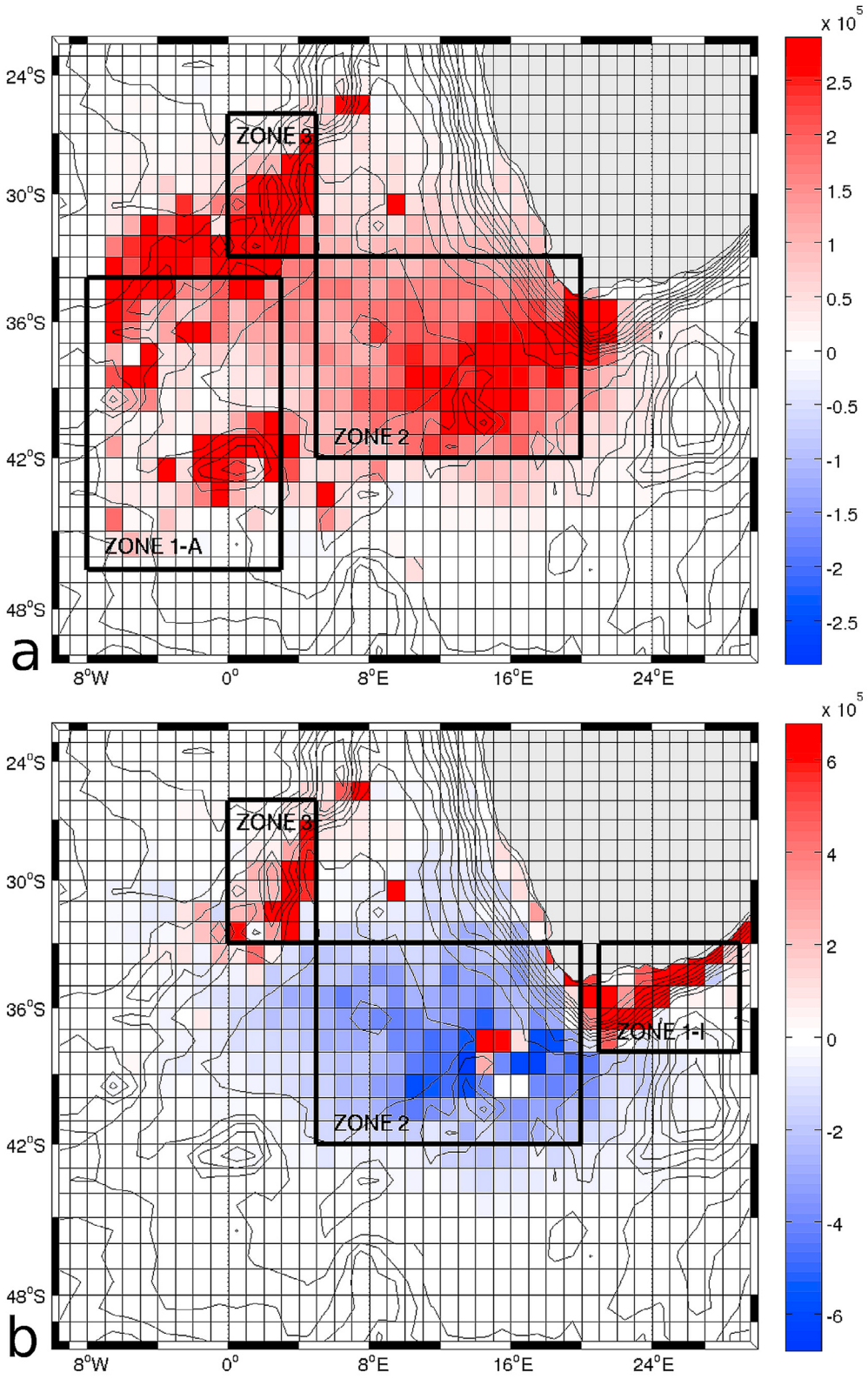

Figure 13. Horizontal mapping (on a 1° × 1° grid) of the salinity gains (red) and losses (blue) experienced along the trajectories associated with the transfer of (a) NA-AAIW and (b) I-AAIW; see text for details on the calculation. Bathymetry contours are drawn in black with a 500 m interval. Four separate zones used to investigate the NA-AAIW and I-AAIW dynamical behavior are delimited (see text for details).

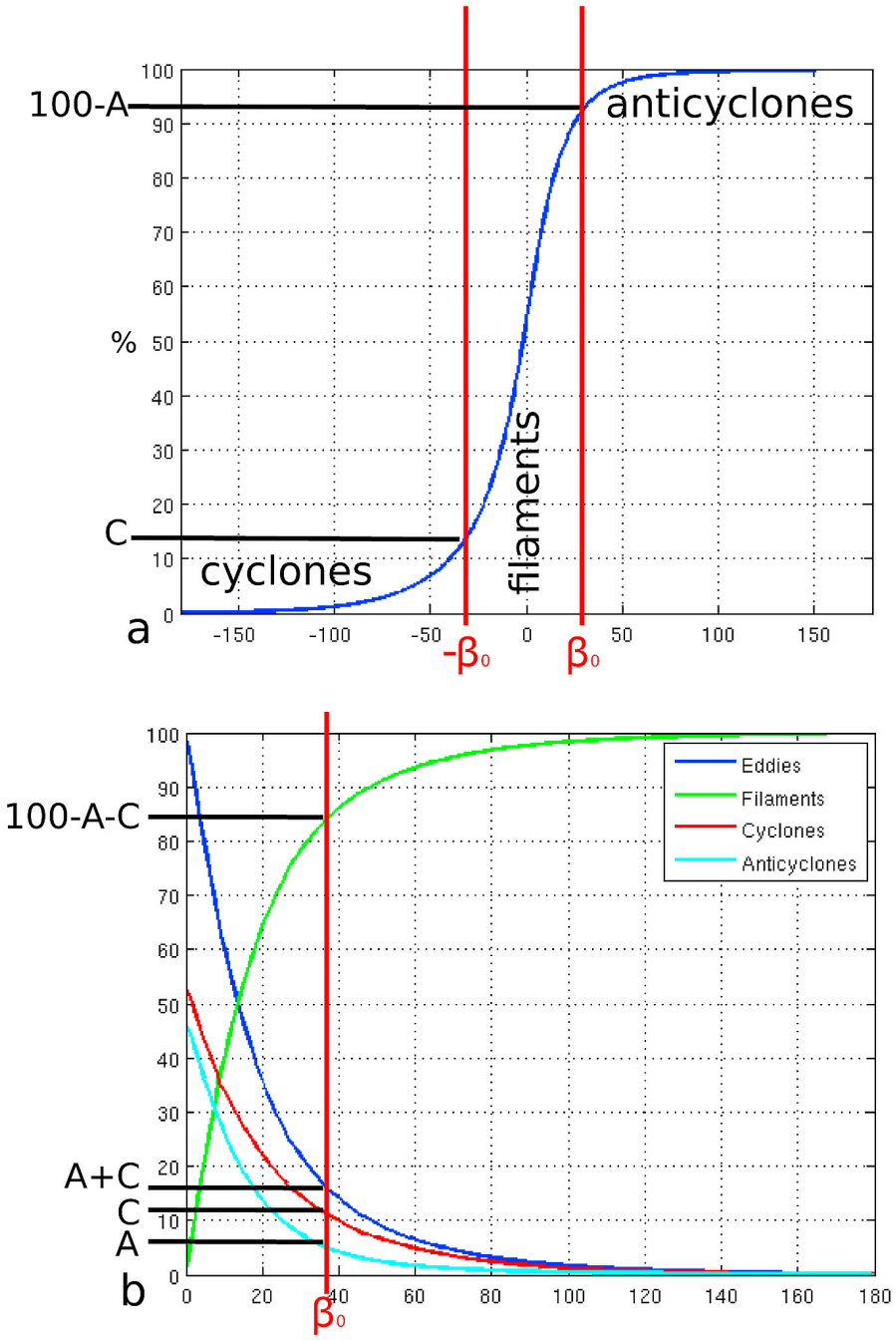

Figure 14. (a) Example of cumulative histogram of the angle variation between successive Lagrangian two-day displacements for all the particles participating in the same transfer, weighted by their transport. β_0 represents a threshold value chosen to distinguish between different dynamics. (b) Schematics showing the percentage of water mass circulation with a specified dynamics, according to the value of β_0 (eddies in dark blue, filaments in green, cyclones in red and anticyclones in blue).

along its journey (Figure 15b). This result is somewhat expected since the I-AAIW is transported by a narrow and intense western-boundary current that does not meander significantly. In the Cape Basin (Zone 2), the contribution of eddies to the I-AAIW transfer is much more marked (Figure 15b: a decrease in the filament contribution—green curves—is necessarily associated with an increase in the eddy contribution). Moreover, in Zone 2 I-AAIW flows more within cyclones than within anticyclones (the red dashed curve lies always above the blue dashed curve). After crossing the Cape Basin, and especially over the Walvis Ridge (Zone 3), the contribution of eddies to the I-AAIW transfer decreases again.

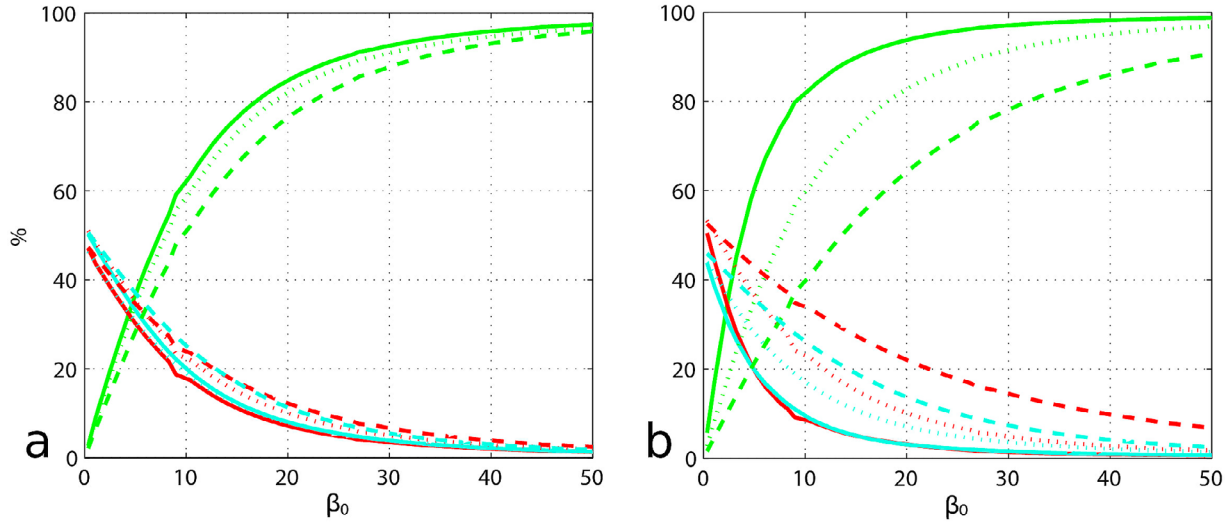

Figure 15. Percentage of filament-like (green curve), cyclonic-like (red) and anticyclonic-like (blue) movements as a function of the critical angle (β_0) chosen to separate them (see text and Figure 15 for details). The horizontal axis is intentionally limited to the range [0 50°]. Results are given upstream the Cape Basin (Zone 1-A or 1-I, solid line), in the Cape Basin (Zone 2, dashed line), and over the Walvis Ridge downstream of the Cape Basin (Zone 3, dotted line), for both AAIW varieties under study: (a) NA-AAIW and (b) I-AAIW.

[45] The proportion of eddy-like behavior obtained for NA-AAIW is almost the same in Zones 1-A and 3 (upstream and downstream the Cape Basin), but is slightly reduced in the Cape Basin (Zone 2) (Figure 15a). It is worth noting that within the Cape Basin, the proportion of NA-AAIW transported in an eddy-like movement is parted equally among cyclonic and anticyclonic rotations (Figure 15a: red and blue curves coincide).

[46] The dynamics of both AAIW varieties evolve differently along their transfer to the NNW section (Figure 16). Zones 1-I and 1-A show the original dynamics of I-AAIW and NA-AAIW, respectively (Figure 16a). Upstream the Cape Basin (Zone 2, Figure 16b), the proportion of eddy-like behavior is much larger for I-AAIW than for NA-AAIW. Over the Walvis Ridge (Zone 3, Figure 16c), the NA-AAIW and I-AAIW varieties are no longer distinguishable by their dynamics and they flow more within filaments than in the Cape Basin.

[47] In conclusion, I-AAIW flows initially more within eddy-like structures (and especially within cyclones) than NA-AAIW in the southeastern Atlantic. In the Cape Basin, both varieties meet and interact, and the differences in

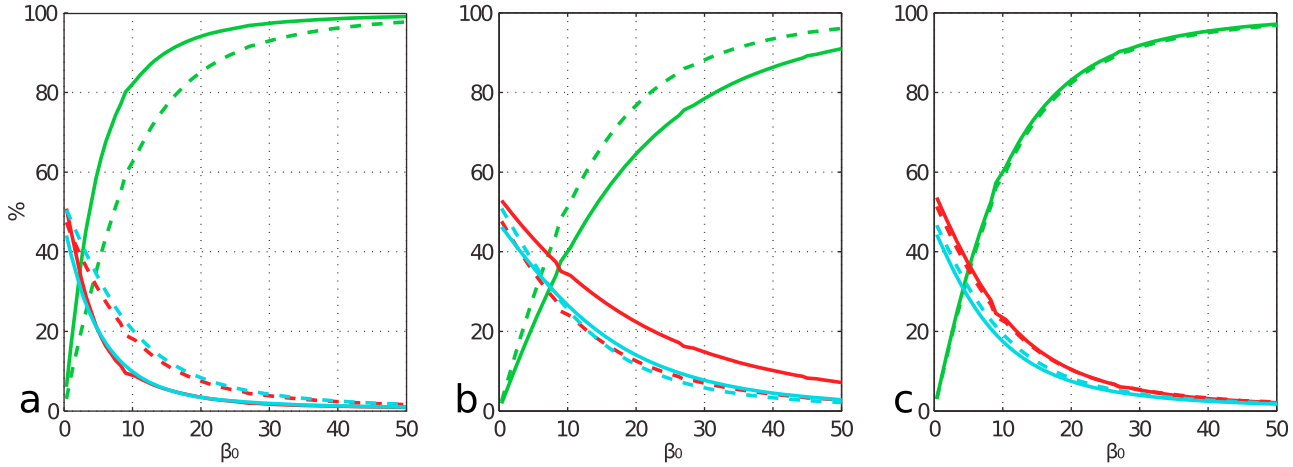

Figure 16. Percentage of filament-like (green curve), cyclonic-like (red) and anticyclonic-like (blue) movements as a function of the critical angle (β_0) chosen to separate them (see text for details). The horizontal axis is intentionally limited to the range [0−50°]. Results for NA-AAIW (dashed line) and I-AAIW (solid line) are given for three typical zones: (a) upstream the Cape Basin (Zone 1-A or 1-I), (b) within the Cape Basin (Zone 2), and (c) over the Walvis Ridge downstream of the Cape Basin (Zone 3).

behavior fade progressively. Over the Walvis Ridge, the NA-AAIW and I-AAIW varieties are no longer distinguishable by their dynamics and they flow more within filaments than in the Cape Basin.

5. Discussion

[48] The large Agulhas Rings generated by the retroflection of the AC define a first mechanism that allows the transfer of warm and salty Indian water to the South Atlantic Ocean [*Gordon*, 1985, 1986]. *Richardson and Garzoli* [2003] confirmed that the AC water that enters the Atlantic Ocean flows over the Walvis Ridge within these anticyclonic rings. Our results confirm that I-AAIW reaches the Walvis Ridge within an eddy-like dynamics. However, our study suggests that I-AAIW is transported by both anticyclonic and cyclonic eddies, with the latter being preponderant. This is in line with the observations by *Arhan et al.* [2011] about I-AAIW captured by cyclonic eddies. Our results indicate also that the I-AAIW transported to the South Atlantic is gradually stirred and then mixed with waters from the SAC. It is rapidly dissociated from eddies as it progresses into the Cape Basin in agreement with results by *McDonagh et al.* [1999]. The resulting water is then exported westward over the Walvis Ridge and forms the Benguela Current as suggested by *Richardson and Garzoli* [2003].

[49] The intermediate water that flows over the Walvis Ridge is a mixture of intermediate water from the AC, the SAC, and the tropical Atlantic [*Richardson and Garzoli*, 2003]. According to *Garzoli and Matano* [2011], water mass transformation occurs everywhere in the oceanic domain around Southern Africa, but is especially intensified in the regions where there is significant mesoscale activity. Our Lagrangian tracking of particles closely related to I-AAIW and A-AAIW shows that changes in the physical properties of both AAIW varieties combine with variability in the Okubo-Weiss parameter, and that the transformations occur mostly in the Cape Basin where the mesoscale activity is known to be strong.

[50] Observations and models show that the Cape Basin is not a passive ocean basin because its dynamics affect significantly the characteristics of the water masses that participate in the AMOC. Moreover, they strongly suggest that this region is essential in connecting the ocean basins and making possible a global circulation [*Garzoli and Matano*, 2011]. The physical properties carried by each AAIW variety have large implications for the stability and variability of the AMOC [*Weijer et al.*, 2002; *Biastoch et al.*, 2009]: the South Atlantic is connected to the Pacific and Indian oceans by the Malvinas Current (the Cold Route) and the Agulhas Current (the Warm Route), respectively [*Gordon*, 1986; *Gordon et al.*, 1992]. *MacDonald and Wunsch* [1996] explained that the warm limb of the AMOC in the South Atlantic is made by both routes of roughly equivalent importance. The Benguela Sources and Transport (BEST) program aimed at determining the variability of the Benguela Current and its origin with current meter moorings deployed along 30°S [*Garzoli and Gordon*, 1996]. One result of the program was that the northward transport in the Benguela Current amounts to 16 Sv, half of which originating in the South Atlantic and a fourth of which in the AC, with the last fourth being a mixture of Atlantic and AC waters [*Garzoli and Gordon*, 1996]. *Gordon* [1986] argued that the thermocline water that comes from the Indian Ocean (the Warm Route) is the main source for the formation of NADW in the North Atlantic. He estimated that the Benguela Current is made of about 65% of the thermocline water and probably 50% of the intermediate water that comes from the Indian Ocean. According to *Sloyan and Rintoul* [2001], the AMOC is closed by cold and relatively fresh intermediate water transformed into warm and salty water under the influence of strong air-sea interactions in the South West Indian Ocean and in the South Atlantic. The thermocline and intermediate waters carried by the SAC and the AC would form the Benguela Current in equal proportions, in agreement with *Schmitz* [1996] who showed an equivalent proportion of Drake Passage and Indian Ocean waters in the origins of this current. However, with the Lagrangian analysis of a global ocean model, *Donners and Drijfhout* [2004] found that 90% of the upper limb of the AMOC comes from the Indian Ocean.

[51] *You* [2002] did not distinguish between the Warm and the Cold Routes for the AAIW that flows in the Benguela Current, but he diagnosed the regions of formation by focusing on physical tracers. He found that 64% of AAIW originates in Drake Passage and 46% in the southwestern Indian Ocean. *You et al.* [2003] confirmed that dAAIW is the dominant source of the Benguela Current: at 6°W and from 34°S to 24°S, the flow of the Benguela Current (12.9 Sv) can be broken up into 80% of dAAIW (10.3 Sv), 11% of siAAIW (1.4 Sv), 3% of Indonesians seas Intermediate Water (0.4 Sv), and 6% of Red Sea Intermediate Water (0.7 Sv). 8.8 Sv out of 10.3 Sv of dAAIW originate directly from the South Atlantic while 1.5 Sv make an incursion in the Indian Ocean. If siAAIW is the dominant origin among the three sources listed in the Indian Ocean, dAAIW remains the main constituent of the Benguela Current, whether it recirculates partly or not in the Indian Ocean [*You et al.*, 2003]. All these results give a very heterogeneous and somewhat contradictory description of the origins of the intermediate waters found in the southeast Atlantic.

[52] Our study suggests that the 12.3 Sv of intermediate water that flow into the Benguela Current are dominated by the South Atlantic variety (9.9 Sv of NA-AAIW, in comparison with only 2.4 Sv of I-AAIW). However, both AAIW varieties undergo fairly important changes in water mass characteristics while entering, progressing across and exiting the Cape Basin. These changes occur where the waters flow over strong topographic features, and inside the Cape Basin where the highly energetic mesoscale and submesoscale dynamics favor an important mixing between the two varieties of intermediate water. The latter result is supported by in situ observations that show vertical fine-scale structures down to the depth of AAIW on profiles located at the edge of eddies [*Piola and Georgi*, 1982; *Gladyshev et al.*, 2008; *Arhan et al.*, 2011]. This suggests that lateral isopycnal mixing develops in the region because of highly nonlinear local dynamics. The effect of topography on eddies and more generally on vertical mixing has not yet been clearly diagnosed and quantified from observations or theoretical process studies, even if it is thought to be important [e.g., *Sutyrin et al.*, 2011; *Jayne et al.*, 2004; *Mauritzen et al.*, 2002].

[53] Whereas successive I-AAIW transformations cancel each other out so that its net changes in properties are not

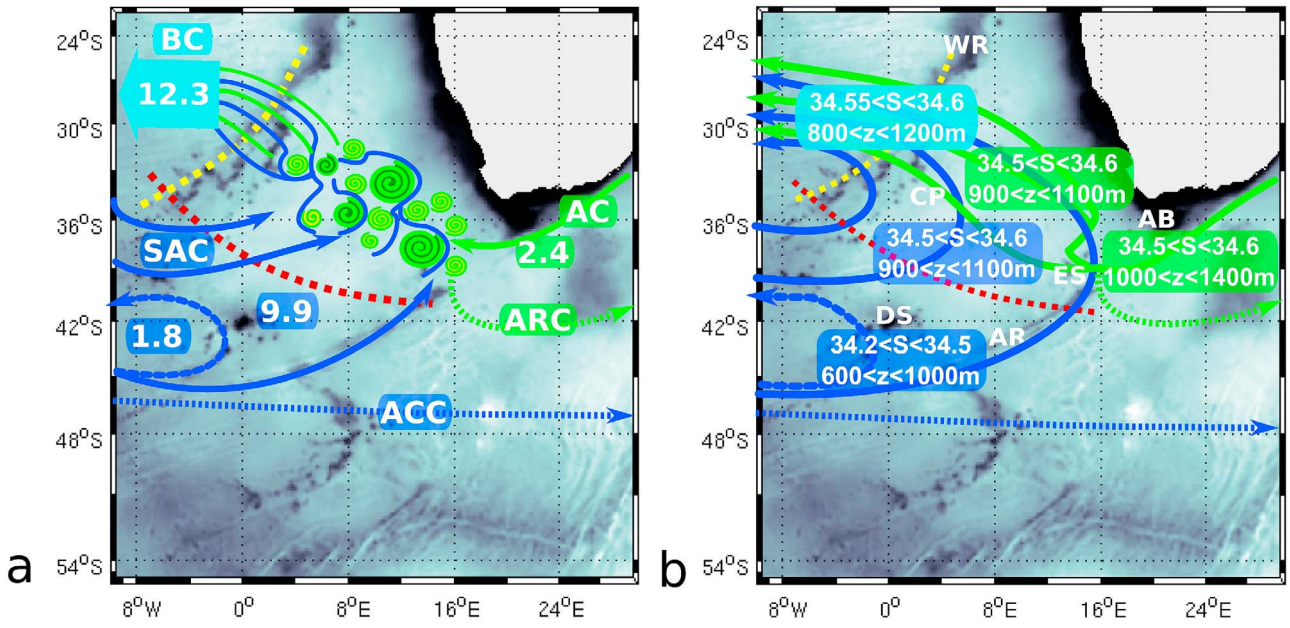

Figure 17. Schematic showing the evolution (a) of the dynamics and (b) of the depth and salinity of the water masses in study. The yellow and red dotted lines show the regions related to salinity increase. I-AAIW is symbolized by the green color. A-AAIW is in blue, with its southern branch shown with a dashed line. Small dotted lines indicate transfers not addressed in this study. The topography is represented by the following acronyms: WR = Walvis Ridge; CP = Cape Basin; ES = Erika Seamounts; AB = Agulhas Bank; AR = Agulhas Ridge; DS = Discovery Seamounts. The currents are represented with their initials, with AAIW transfers expressed in sverdrups: AC = Agulhas Current; SAC = South Atlantic Current; ACC = Antarctic Circumpolar Current; ARC = Agulhas Retroflection Current; BC = Benguela Current.

significant overall, this is not true for the Atlantic variety. Indeed, NA-AAIW has to flow over the steep topographic features of the RSA and Discovery seamounts as well as of the Agulhas Ridge before entering the Cape Basin. These crossings are accompanied by a significant increase of the salinity of the water mass. Inside the Cape Basin, NA-AAIW and I-AAIW are stirred together by the complex local nonlinear dynamics: NA-AAIW gets saltier while I-AAIW gets fresher. Both varieties exit the Cape Basin by flowing over the Walvis Ridge where they both get saltier. Hence, downstream the Walvis Ridge where the two varieties are part of the Benguela Current, NA-AAIW has become saltier than at its origins, while I-AAIW salinity is comparable to its initial range.

[54] Therefore, even if the dominating variety of intermediate water in the interocean exchange of AAIW is the Atlantic one, our study suggests that its physical properties are strongly changed during its journey across the Cape Basin: northwest of the Walvis Ridge, the A-AAIW and I-AAIW varieties are no longer distinguishable in terms of salinity and depth ranges. The Cape Basin region has to be considered as an active region with regard to water mass transformation.

6. Conclusions

[55] Our study aimed at characterizing the origin, properties, transfers, dynamics, and transformations of different varieties of Antarctic Intermediate Water (AAIW) present in the Cape Basin region of the South Atlantic until their confluence into the Benguela Current. A regional numerical simulation, run at high temporal and spatial resolution in the ocean domain around Southern Africa, made possible the calculation of maps, vertical profiles, and potential temperature versus salinity diagrams to identify different AAIW varieties. The diagnostic tool ARIANE provided a Lagrangian interpretation of the model results. This allowed us to quantify the intensity of some water mass transfers and to illustrate the dynamics and transformations inherent to these transfers.

[56] In this study, we compared our results about salinity, depth and density with available in situ measurements (profiling Argo floats and GoodHope data) and other published studies. Then, we computed the Okubo-Weiss parameter and the change in the direction of the Lagrangian velocity to determine whether the circulation is achieved preferentially within eddies or filaments. Three varieties of AAIW (characterized by a salinity minimum below the thermocline) converge in the southeast Atlantic from the South Atlantic and the Indian Ocean. The evolution of their dynamical and physical properties along their pathways is summarized in Figure 17. Our simulation shows that AAIW flows from the South Atlantic within the SAC between 600 and 1000 m, with inflowing salinity less than 34.5 (A-AAIW, 11.7 Sv). This water mass separates into two branches. A southern variety (SA-AAIW, 1.8 Sv) recirculates rapidly westward, blocked by the steep topography that separates the southern portion of the Cape Basin from the South Atlantic. The remainder (NA-AAIW, 9.9 Sv) does cross the Cape

Basin and joins the Benguela Current, flowing over the Walvis Ridge. During its journey, its physical characteristics are modified by mixing with surrounding waters (which are saltier), in association with topographical interactions and mesoscale/submesoscale dynamics. The AAIW with an Indian Ocean origin (I-AAIW, 2.4 Sv) flows within the AC between 1000 and 1400 m depth, with salinity greater than 34.5. It experiences upwelling in the Cape Basin. Up to the Walvis Ridge, I-AAIW flows more within eddies, especially within cyclones, than NA-AAIW. There, both varieties merge and flow together in the Benguela Current, as SEA-AAIW. They fill a layer from 800 to 1100 m depth and have salinity varying between 34.55 and 34.6. The water mass properties derived from the model are close to those observed, despite a +0.2 mean bias of the salinity minimum.

[57] Our model-based estimates of the AAIW contribution to the Benguela Current complement a rich range of values in other published studies. The very high mesoscale and submesoscale activity that develops in the Cape Basin explains easily the difficulty of a thorough and accurate quantification of the AAIW varieties as their physical properties are rapidly mixed and deviate from their original characteristics [*Richardson and Garzoli*, 2003; *Boebel et al.*, 2003]. Our calculations underline the crucial role of small-scale dynamical processes (eddies, fronts, and filaments) on the structure of interbasin transfers south of Africa. Our numerical study provides new information about the dynamics of AAIW around Southern Africa. Some processes such as the increase of salinity in specific areas of the studied domain (for instance along the continental slope of the Agulhas Bank) are still under investigation. Understanding them asks for a careful inspection of the physics at work in the regional ocean model and must probably be achieved online, which is beyond the scope of this study.

[58] **Acknowledgments.** We thank Alberto Piola, Frank Shillington, a third anonymous reviewer, and the Editor, Des Barton, for helpful and detailed comments. We are especially grateful to Emanuela Rusciano for fruitful discussions and for providing us with some of her analyses, which are part of a paper currently submitted.

References

Arhan, M., S. Speich, C. Messager, G. Dencausse, R. Fine, and M. Boye (2011), Anticyclonic and cyclonic eddies of subtropical origin in the subantarctic zone south of Africa, *J. Geophys. Res.*, *116*, C11004, doi:10.1029/2011JC007140.

Ayina, H.-L., A. Bentamy, A. M. Mestas-Nuñez, and G. Madec (2006), The impact of satellite winds and latent heat fluxes in a numerical simulation of the tropical Pacific Ocean, *J. Clim.*, *19*, 5889–5902, doi:10.1175/JCLI3939.1.

Belkin, I. M., and A. L. Gordon (1996), Southern Ocean fronts from the Greenwich meridian to Tasmania, *J. Geophys. Res.*, *101*(C2), 3675–3696, doi:10.1029/95JC02750.

Bentamy, A., K. B. Katsaros, M. Alberto, W. M. Drennan, E. B. Forde, and H. Roquet (2003), Satellite estimates of wind speed and latent heat flux over the global oceans, *J. Clim.*, *16*, 637–656, doi:10.1175/1520-0442(2003)016<0637:SEOWSA>2.0.CO;2.

Beron-Vera, F. J., M. J. Olascoaga, and G. J. Goni (2008), Oceanic mesoscale eddies as revealed by Lagrangian coherent structures, *Geophys. Res. Lett.*, *35*, L12603, doi:10.1029/2008GL033957.

Biastoch, A., C. W. Böning, R. U. Schwarzkopf, and J. R. E. Lutjeharms (2009), Increase in Agulhas leakage due to poleward shift of Southern Hemisphere westerlies, *Nature*, *462*, 495–498, doi:10.1038/nature08519.

Blanke, B., and S. Raynaud (1997), Kinematics of the Pacific Equatorial Undercurrent: An Eulerian and Lagrangian approach from GCM results, *J. Phys. Oceanogr.*, *27*, 1038–1053, doi:10.1175/1520-0485(1997)027<1038:KOTPEU>2.0.CO;2.

Blanke, B., M. Arhan, G. Madec, and S. Roche (1999), Warm water paths in the Equatorial Atlantic as diagnosed with a general circulation model, *J. Phys. Oceanogr.*, *29*, 2753–2768, doi:10.1175/1520-0485(1999)029<2753:WWPITE>2.0.CO;2.

Boebel, O., J. R. E. Lutjeharms, C. Schmid, C. Zenk, T. Rossby, and C. Barron (2003), The Cape Cauldron: A regime of turbulent inter-ocean exchange, *Deep Sea Res., Part I*, *50*, 57–86, doi:10.1016/S0967-0645(02)00379-X.

Böning, C. W., A. Dispert, M. Visbeck, S. R. Rintoul, and F. U. Schwarzkopf (2008), The response of the Antarctic Circumpolar Current to recent climate change, *Nat. Geosci.*, *1*, 864–869, doi:10.1038/ngeo362.

Broecker, W. S. (1987), The biggest chill, *Nat. Hist. Mag.*, *47*, 74–82.

Broecker, W. S. (1991), The Great Conveyor Belt, *Oceanography*, *4*, 79–89.

Carton, J. A., and B. S. Giese (2008), A reanalysis of ocean climate using Simple Ocean Data Assimilation (SODA), *Mon. Weather Rev.*, *136*, 2999–3017, doi:10.1175/2007MWR1978.1.

d'Ovidio, F., V. Fernandez, E. Hernandez-Garcia, and C. Lopez (2004), Mixing structures in the Mediterranean Sea from finite-size Lyapunov exponents, *Geophys. Res. Lett.*, *31*, L17203, doi:10.1029/2004GL020328.

de Ruijter, W. P. M., A. Biastoch, S. S. Drijfhout, J. R. E. Lutjeharms, R. P. Matano, T. Pichevin, P. J. Van Leeuwen, and W. Weijer (1999), Indian-Atlantic interocean exchange: Dynamics, estimation and impact, *J. Geophys. Res.*, *104*, 20,885–20,910, doi:10.1029/1998JC900099.

Dencausse, G., M. Arhan, and S. Speich (2010), Spatio-temporal characteristics of the Agulhas Current retroflection, *Deep Sea Res., Part I*, *57*(11), 1392–1405, doi:10.1016/j.dsr.2010.07.004.

Dencausse, G., M. Arhan, and S. Speich (2011), Is there a continuous Subtropical Front south of Africa?, *J. Geophys. Res.*, *116*, C02027, doi:10.1029/2010JC006587.

Donners, J., and S. S. Drijfhout (2004), The Lagrangian view of South Atlantic interocean exchange in a global ocean model compared with inverse model results, *J. Phys. Oceanogr.*, *34*, 1019–1035, doi:10.1175/1520-0485(2004)034<1019:TLVOSA>2.0.CO;2.

Ducet, N., P. Le Traon, and G. Reverdin (2000), Global high-resolution mapping of ocean circulation from TOPEX/POSEIDON and ERS-1 and -2, *J. Geophys. Res.*, *105*, 19,477–19,498, doi:10.1029/2000JC900063.

Duncan, C. P. (1970), The Agulhas Current, MS thesis, 76 pp., Univ. of Hawai'i at Mānoa, Honolulu.

Garzoli, S. L., and A. L. Gordon (1996), Origins and variability of the Benguela Current, *J. Geophys. Res.*, *101*, 897–906, doi:10.1029/95JC03221.

Garzoli, S. L., and R. Matano (2011), The South Atlantic and the Atlantic Meridional Overturning Circulation, *Deep Sea Res., Part II*, *58*, 1837–1847, doi:10.1016/j.dsr2.2010.10.063.

Gladyshev, S., M. Arhan, A. Sokov, and S. Speich (2008), A hydrographic section from South Africa to the southern limit of the Antarctic Circumpolar Current at the Greenwich meridian, *Deep Sea Res., Part I*, *55*(10), 1284–1303, doi:10.1016/j.dsr.2008.05.009.

Gordon, A. L. (1985), Indian-Atlantic transfer of thermocline water at the Agulhas retroflection, *Science*, *227*, 1030–1033, doi:10.1126/science.227.4690.1030.

Gordon, A. L. (1986), Interocean exchange of thermocline water, *J. Geophys. Res.*, *91*, 5037–5046, doi:10.1029/JC091iC04p05037.

Gordon, A. L. (2001), Interocean exchange, in *Ocean Circulation and Climate*, *Int. Geophys. Ser.*, vol. 77, edited by G. Siedler, J. Church, and J. Gould, chap. 4.7, pp. 303–314, Academic, San Diego, Calif.

Gordon, A. L. (2003), The brawniest retroflection, *Nature*, *421*(6926), 904–905, doi:10.1038/421904a.

Gordon, A. L., R. F. Weiss, W. M. Smethie Jr., and M. J. Warner (1992), Thermocline and intermediate water communication between the South Atlantic and Indian Oceans, *J. Geophys. Res.*, *97*, 7223–7240, doi:10.1029/92JC00485.

Hallberg, R. W., and A. Gnanadesikan (2006), On methods for solving the oceanic equations of motion in generalized vertical coordinates, *Ocean Modell.*, *11*(1–2), 224–233.

Hanawa, K., and L. D. Talley (2001), Mode water, in *Ocean Circulation and Climate*, *Int. Geophys. Ser.*, vol. 77, edited by G. Siedler, J. Church, and J. Gould, chap. 5.4, pp. 373–386, Academic, San Diego, doi:10.1016/S0074-6142(01)80129-7.

Institut Français de Recherche Pour l'Exploitation de la Mer and Centre ERS d'Archivage et de Traitement (2002), QuikSCAT scatterometer mean wind field products user manual, version 1.0, *Rep. C2-MUT-W-04-IF*, Plouzané, France.

Ito, T., P. Parekh P., S. Dutkiewicz, and M. J. Follows (2005), The Antarctic Circumpolar Productivity Belt, *Geophys. Res. Lett.*, *32*, L13604, doi:10.1029/2005GL023021.

Jacobs, S. S., and D. T. Georgi (1977), Observations on the southwest Indian/Antarctic Ocean, in *A Voyage of Discovery*, edited by M. Angel, pp. 43–84, Pergamon, Oxford, U. K.

Jayne, S. R., L. C. St. Laurent, and S. T. Gille (2004), Connections between ocean bottom topography and Earth's climate, *Oceanography*, *17*(1), 65–74, doi:10.5670/oceanog.2004.68.

Lumpkin, R., and K. Speer (2007), Global Ocean meridional overturning, *J. Phys. Oceanogr.*, *37*, 2550–2562, doi:10.1175/JPO3130.1.

Lumpkin, R., K. Speer, and K. P. Kolterman (2008), Transport across 48°N in the Atlantic Ocean, *J. Phys. Oceanogr.*, *38*, 733–752, doi:10.1175/2007JPO3636.1.

Lutjeharms, J. R. E. (2001), The Agulhas Current, in *Encyclopedia of Ocean Sciences*, edited by J. H. Steele, S. A. Thorpe, and K. K. Turekian, pp. 104–113, Academic, San Diego, doi:10.1006/rwos.2001.0365.

Lutjeharms, J. R. E. (2006), *The Agulhas Current*, 329 pp., Springer, Heidelberg, Germany.

Lutjeharms, J. R. E., O. Boebel, and H. T. Rossby (2003), Agulhas cyclones, *Deep Sea Res., Part II*, *50*, 13–34, doi:10.1016/S0967-0645(02)00378-8.

MacDonald, A., and C. Wunsch (1996), The global ocean circulation and heat flux, *Nature*, *382*, 436–439, doi:10.1038/382436a0.

Mauritzen, C., K. L. Polzin, M. S. McCartney, R. C. Millard, and D. E. West-Mack (2002), Evidence in hydrography and density fine structure for enhanced vertical mixing over the Mid-Atlantic Ridge in the western Atlantic, *J. Geophys. Res.*, *107*(C10), 3147, doi:10.1029/2001JC001114.

McCartney, M. S. (1977), Subantarctic Mode Water, in *A Voyage of Discovery: George Deacon 70th Anniversary Volume*, edited by M. V. Angel, pp. 103–119, Pergamon, Oxford, U. K.

McDonagh, E. L., K. J. Heywood, and M. P. Meredith (1999), On the structure, paths, and fluxes associated with Agulhas Rings, *J. Geophys. Res.*, *104*, 21,007–21,020, doi:10.1029/1998JC900131.

Okubo, A. (1970), Horizontal dispersion of floatable particles in the vicinity of velocity singularities such as convergences, *Deep Sea Res.*, *17*, 445–454.

Olbers, D., D. Borowski, C. Völker, and J. O. Wölff (2004), The dynamical balance, transport and circulation of the Antarctic Circumpolar Current, *Antarct. Sci.*, *16*, 439–470, doi:10.1017/S0954102004002251.

Orsi, A. H., T. Whitworth III, and W. D. Nowlin Jr. (1995), On the meridional extent and fronts of the Antarctic Circumpolar Current, *Deep Sea Res.*, *42*, 641–673, doi:10.1016/0967-0637(95)00021-W.

Penven, P., C. Roy, J. R. E. Lutjeharms, A. Colin de Verdière, A. Johnson, F. Shillington, P. Fréon, and G. Brundrit (2001), A regional hydrodynamic model of the Southern Benguela, *S. Afr. J. Sci.*, *97*, 472–476.

Penven, P., P. Marchesiello, L. Debreu, and J. Lefèvre (2008), Software tools for pre- and post-processing of oceanic regional simulations, *Environ. Modell. Software*, *23*, 660–662, doi:10.1016/j.envsoft.2007.07.004.

Peterson, R. G., and L. Stramma (1991), Upper-level circulation in the South Atlantic Ocean, *Prog. Oceanogr.*, *26*, 1–73, doi:10.1016/0079-6611(91)90006-8.

Piola, A. R., and D. T. Georgi (1982), Circumpolar properties of Antarctic Intermediate Water and Subantarctic Mode Water, *Deep Sea Res.*, *29*, 687–711, doi:10.1016/0198-0149(82)90002-4.

Piola, A. R., and A. L. Gordon (1989), Intermediate waters in the southwest South Atlantic, *Deep Sea Res., Part A*, *36*(1), 1–16, doi:10.1016/0198-0149(89)90015-0.

Pollard, R. T., M. I. Lucas, and J. F. Read (2002), Physical controls on biogeochemical zonation in the Southern Ocean, *Deep Sea Res., Part II*, *49*, 3289–3305, doi:10.1016/S0967-0645(02)00084-X.

Reid, J. L. (1989), On the total geostrophic circulation of the South Atlantic Ocean: Flow patterns, tracers, and transports, *Prog. Oceanogr.*, *23*, 149–244, doi:10.1016/0079-6611(89)90001-3.

Richardson, P. L., and S. L. Garzoli (2003), Characteristics of intermediate water flow in the Benguela Current as measured with RAFOS floats, *Deep Sea Res., Part II*, *50*, 87–118, doi:10.1016/S0967-0645(02)00380-6.

Rintoul, S. R., C. Hughes, and D. Olbers (2001), The Antarctic Circumpolar System, in *Ocean Circulation and Climate*, *Int. Geophys. Ser.*, vol. 77, edited by G. Siedler, J. Church, and J. Gould, pp. 271–302, Academic, San Diego, Calif., doi:10.1016/S0074-6142(01)80124-8.

Sadarjoen, I. A., and F. H. Post (2000), Detection, quantification, and tracking of vortices using streamline geometry, *Comput. Graph.*, *24*, 333–341, doi:10.1016/S0097-8493(00)00029-7.

Sarmiento, J. L., N. Gruber, M. A. Brzezinksi, and J. P. Dunne (2004), High latitude controls of thermocline nutrients and low latitude biological productivity, *Nature*, *426*, 56–60, doi:10.1038/nature02127.

Schmid, C., and S. L. Garzoli (2009), New observations of the spreading and variability of the Antarctic Intermediate Water in the Atlantic, *J. Mar. Res.*, *67*, 815–843, doi:10.1357/002224009792006151.

Schmitz, W. J. (1996), On the world ocean circulation: Volume 1. Some global features/North Atlantic Circulation, *Tech. Rep. WHOI-96-03*, 141 pp., Woods Hole Oceanogr. Inst., Woods Hole, Mass.

Shchepetkin, A. F., and J. C. McWilliams (2005), The regional oceanic modeling system (ROMS): A split-explicit, free-surface, topography following- coordinate oceanic model, *Ocean Modell.*, *9*, 347–404, doi:10.1016/j.ocemod.2004.08.002.

Shchepetkin, A. F., and J. C. McWilliams (2009), Correction and commentary for "Ocean forecasting in terrain-following coordinates: Formulation and skill assessment of the regional ocean modeling system" by Haidvogel et al., *J. Comput. Phys.*, *227*, 3595–3624.

Sievers, H. A., and W. D. Nowlin (1984), The stratification of water masses of Drake Passage, *J. Geophys. Res.*, *89*, 10,489–10,514, doi:10.1029/JC089iC06p10489.

Sloyan, B. M., and S. R. Rintoul (2001), Circulation, renewal and modification of Antarctic Mode and Intermediate Water, *J. Phys. Oceanogr.*, *31*, 1005–1030, doi:10.1175/1520-0485(2001)031<1005:CRAMOA>2.0.CO;2.

Smith, W. H. F., and D. T. Sandwell (1997), Global seafloor topography from satellite altimetry and ship depth soundings, *Science*, *277*, 1956–1962, doi:10.1126/science.277.5334.1956.

Sokolov, S., and S. R. Rintoul (2002), Structure of Southern Ocean fronts at 140°E, *J. Mar. Syst.*, *37*(1–3), 151–184, doi:10.1016/S0924-7963(02)00200-2.

Sokolov, S., and S. R. Rintoul (2007), On the relationship between fronts of the Antarctic Circumpolar Current and surface chlorophyll concentrations in the Southern Ocean, *J. Geophys. Res.*, *112*, C07030, doi:10.1029/2006JC004072.

Sokolov, S., and S. R. Rintoul (2009a), Circumpolar structure and distribution of the Antarctic Circumpolar Current fronts: 1. Mean circumpolar paths, *J. Geophys. Res.*, *114*, C11018, doi:10.1029/2008JC005108.

Sokolov, S., and S. R. Rintoul (2009b), Circumpolar structure and distribution of the Antarctic Circumpolar Current fronts: 2. Variability and relationship to sea surface height, *J. Geophys. Res.*, *114*, C11019, doi:10.1029/2008JC005248.

Souza, J. M. A. C., C. de Boyer Montegut, and P. Y. Le Traon (2011), Comparison between three implementations of automatic identification algorithms for the quantification and characterization of mesoscale eddies in the South Atlantic Ocean, *Ocean Sci.*, *7*, 317–334, doi:10.5194/os-7-317-2011.

Speich, S., B. Blanke, and G. Madec (2001), Warm and cold water paths of an O.G.C.M. thermohaline conveyor belt, *Geophys. Res. Lett.*, *28*, 311–314, doi:10.1029/2000GL011748.

Speich, S., J. R. E. Lutjeharms, P. Penven, and B. Blanke (2006), Role of bathymetry in Agulhas Current configuration and behaviour, *Geophys. Res. Lett.*, *33*, L23611, doi:10.1029/2006GL027157.

Speich, S., B. Blanke, and W. Cai (2007), Atlantic meridional overturning and the Southern Hemisphere supergyre, *Geophys. Res. Lett.*, *34*, L23614, doi:10.1029/2007GL031583.

Speich, S., M. Arhan, E. Rusciano, V. Faure, M. Ollitrault, A. Prigent, and S. Swart (2012), Use of ARGO floats to study the ocean dynamics south of Africa: What we have learned from the GoodHope project and what we plan within the SAMOC International Programme, *Joint Coriolis Mercator Ocean Q. Newsl.*, *45*, 21–27.

Stramma, L., and M. England (1999), On the water masses and mean circulation of the South Atlantic Ocean, *J. Geophys. Res.*, *104*, 20,863–20,884, doi:10.1029/1999JC900139.

Sutyrin, G., S. Herbette, and X. Carton (2011), Deformation and splitting of baroclinic eddies encountering a tall seamount, *Geophys. Astrophys. Fluid Dyn.*, *105*(4–5), 478–505, doi:10.1080/03091929.2011.566566.

Talley, L. D. (1996), Antarctic Intermediate Water in the South Atlantic, in *The South Atlantic: Present and Past Circulation*, edited by G. Wefer et al., pp. 219–238, Springer, Berlin, doi:10.1007/978-3-642-80353-6_11.

Toggweiler, J. R., and B. Samuels (1998), On the ocean's large-scale circulation near the limit of no vertical mixing, *J. Phys. Oceanogr.*, *28*, 1832–1852, doi:10.1175/1520-0485(1998)028<1832:OTOSLS>2.0.CO;2.

Watson, A. J., and A. C. N. Garabato (2006), The role of Southern Ocean mixing and upwelling in glacial-interglacial atmospheric CO_2 change, *Tellus, Ser. B*, *58*, 73–87.

Weijer, W., W. P. M. de Ruijter, A. Sterl, and S. S. Drijfhout (2002), Response of the Atlantic overturning circulation to South Atlantic sources of buoyancy, *Global Planet. Change*, *34*, 293–311, doi:10.1016/S0921-8181(02)00121-2.

Weiss, J. (1991), The dynamics of enstrophy transfer in two-dimensional hydrodynamics, *Physica D*, *48*(2–3), 273–294, doi:10.1016/0167-2789(91)90088-Q.

You, Y. (2002), Quantitative estimate of Antarctic Intermediate Water contributions from the Drake Passage and the southwest Indian Ocean to the South Atlantic, *J. Geophys. Res.*, *107*(C4), 3031, doi:10.1029/2001JC000880.

You Y., J. R. E. Lutjeharms, O. Boebel, and W. P. M. de Ruijter (2003), Quantification of the interocean exchange of intermediate water masses around southern Africa, *Deep Sea Res., Part II*, *50*, 197–228, doi:10.1016/S0967-0645(02)00384-3.